

Uncertainties of Satellite-based Essential Climate Variables from Deep Learning

Junyang Gou^{1*}, Arnt-Børre Salberg², Mostafa Kiani Shahvandi¹,
 Mohammad J. Tourian³, Ulrich Meyer⁴, Eva Boergens⁵,
 Anders U. Waldeland², Isabella Velicogna^{6,7}, Fredrik Dahl²,
 Adrian Jäggi⁴, Konrad Schindler¹, Benedikt Soja¹

¹Institute of Geodesy and Photogrammetry, ETH Zurich.

²Norwegian Computing Center.

³Institute of Geodesy, University of Stuttgart.

⁴Astronomical Institute, University of Bern.

⁵Department 1: Geodesy, Section 1.3: Earth System Modelling, GFZ
 Helmholtz Centre for Geosciences.

⁶Department of Earth System Science, University of California Irvine.

⁷Jet Propulsion Laboratory, California Institute of Technology.

*Corresponding author(s). E-mail(s): jungou@ethz.ch;

Contributing authors: salberg@nr.no; mkiani@ethz.ch;

tourian@gis.uni-stuttgart.de; ulrich.meyer@unibe.ch;

eva.boergens@gfz-potsdam.de; andersuw@nr.no; isabella@uci.edu;

fadahl@nr.no; adrian.jaeggi@unibe.ch; schindler@ethz.ch; soja@ethz.ch;

Abstract

Accurate uncertainty information associated with essential climate variables (ECVs) is crucial for reliable climate modeling and understanding the spatiotemporal evolution of the Earth system. In recent years, geoscience and climate scientists have benefited from rapid progress in deep learning to advance the estimation of ECV products with improved accuracy. However, the quantification of uncertainties associated with the output of such deep learning models has yet to be thoroughly adopted. This survey explores the types of uncertainties associated with ECVs estimated from deep learning and the techniques to quantify them. The focus is on highlighting the importance of quantifying uncertainties inherent in ECV estimates, considering the dynamic and multifaceted nature of climate data. The survey starts by clarifying the definition of aleatoric and epistemic

uncertainties and their roles in a typical satellite observation processing workflow, followed by bridging the gap between conventional statistical and deep learning views on uncertainties. Then, we comprehensively review the existing techniques for quantifying uncertainties associated with deep learning algorithms, focusing on their application in ECV studies. The specific need for modification to fit the requirements from both the Earth observation side and the deep learning side in such interdisciplinary tasks is discussed. Finally, we demonstrate our findings with two ECV examples, snow cover and terrestrial water storage, and provide our perspectives for future research.

Keywords: deep learning, uncertainty quantification, essential climate variables, satellite observations, snow cover, terrestrial water storage

Highlights

- Comprehensive review of uncertainty quantification approaches using deep learning applied to earth observation data and essential climate variables (ECVs).
- Discuss and bridge the gap between deep learning and conventional statistical perspectives on uncertainties.
- Demonstrate the efficiency of deep learning uncertainty quantification approaches with example use cases for two selected ECVs: snow cover and terrestrial water storage changes.
- Provide recommendations for geoscience and climate scientists to accurately quantify uncertainties when applying deep learning techniques.

1 Introduction

The Earth’s climate system has been evolving rapidly in recent years, leading to more frequent climate extremes (AghaKouchak et al, 2020; Rodell and Li, 2023) and pressing needs for systematic observations of critical climate variables. To establish a sustainable climate monitoring system, the Global Climate Observing System (GCOS) program developed the concept of “Essential Climate Variables” (ECVs; Zemp et al 2022), which provide fundamental observational requirements to document and understand climate change, constrain climate prediction, and inform policy decisions on climate adaptation and mitigation (Bojinski et al, 2014). ECVs are monitored using satellite systems, ground-based, ocean-based, and atmospheric sensors and form the basis for defining science requirements of observational programs of the Earth system (Bayat et al, 2021). Unfortunately, not all ECVs can be observed cost-effectively, and some are not even directly observable (Bojinski et al, 2014). Moreover, the current observing systems for most ECVs cannot fulfill the defined ideal or intermediate requirements in terms of spatio-temporal resolution and/or accuracy. The observations may be sporadic, not acquired frequently enough, of limited accuracy, or even entirely missing over parts of the Earth system. For climate studies, the measurements need to be conducted over long time scales (decades to multiple decades), continuously, comprehensively, systematically, and globally. To this end, satellite Earth observation (sEO) data have played a critical role and have truly improved the availability and quality of observations of ECVs (Anderson et al, 2017).

Due to the complex nature of the Earth system and our inevitably incomplete knowledge of it, data-driven methods play an important role in estimating ECVs (e.g., Wylie et al, 2007; Dangendorf et al, 2021; Gou and Tourian, 2022). Such methods become more promising with the recent progress in deep learning, which have significant potential for improving the quality of observations and models of the Earth’s climate system (Reichstein et al, 2019; Schneider et al, 2023), especially when applied to data from sEO techniques, which have been providing a vast amount of observations of the Earth (Zhu et al, 2017). Deep learning approaches have achieved remarkable success in various fields of satellite-based climate monitoring, including pattern recognition, spatio-temporal downscaling, and quantitative analysis (Yuan et al, 2020). Their value and further potential have been widely recognized by geoscience and climate scientists for ECV retrievals. Many studies successfully applied deep learning techniques to various ECVs in various domains of Earth science, often with unprecedented efficiency and accuracy. However, uncertainty quantification is still missing in many studies (see, e.g., Jeppesen et al, 2019; Segal-Rozenhaimer et al, 2020; Liu et al, 2020; Li et al, 2022c, and Table 1), which has been defined as a critical next step by some pioneering studies (Lam et al, 2023; Zhang et al, 2023; Price et al, 2023).

Realistic uncertainty information is crucial for interpreting or predicting changes in the climate system and, in turn, provides confidence levels for forecasts used by decision makers (Reilly et al, 2001; Smith and Stern, 2011). Such uncertainties are necessary for most, if not all, further investigations based on ECV datasets, such as assimilating data into models (e.g., Schumacher et al, 2016; De Lannoy et al, 2019; Giroto et al, 2020; Luo et al, 2023; Gerdener et al, 2023), data fusion (e.g., Tourian et al, 2023), or extreme event and time series analysis (Hoffmann et al, 2020;

Laimighofer and Laaha, 2022; Saemian et al, 2024). Multiple ECVs may be combined to derive the target parameter of interest, such as the groundwater storage changes obtained by combining multiple other satellite-based ECVs (Güntner et al, 2024). In this case, the uncertainties of the different input data sets and their harmonization are fundamentally important. Unsatisfactory uncertainty estimates pose a significant challenge in using currently available ECV products (Soltani et al, 2021).

However, applying appropriate deep learning approaches to quantify realistic uncertainty information in estimating ECVs based on real-world sEO data is challenging. Gawlikowski et al (2023) categorize the uncertainties into three sources: data acquisition, deep learning model design and training, and inference. Most of the efforts so far have been dedicated to quantifying the uncertainties related to model architecture and training (Abdar et al, 2021), but have largely ignored (or only implicitly considered) the uncertainties related to data acquisition or during inference (He and Jiang, 2023), since the latter are not dominating in classical vision or language modeling tasks that motivated the recent revolution of deep learning techniques. However, uncertainties originating from data acquisition or inference processes are crucial for satellite data and are the keys to providing realistic uncertainty information for sEO-derived ECVs. The high variability of the real world needs to be taken into account. Otherwise, it will introduce significant distribution shifts in the data (Gawlikowski et al, 2023). Nevertheless, EO satellites usually have multiple measurement systems with assorted characteristics onboard, the inherent noise of which needs to be characterized (Chuvienco, 2020). Another major barrier is the lack of ground truth, prohibiting us from performing uncertainty calibration/validation based on the information contained in a validation dataset (Kuleshov et al, 2018). This very problem poses a great challenge in validating satellite-based ECVs (Bayat et al, 2021). Furthermore, it is questionable whether the purely statistical deep learning paradigm is sufficient to quantify uncertainties related to physical domain knowledge, especially the unknown part of the total uncertainty (Povey and Grainger, 2015a). In summary, we need to pay attention to the special requirements for the task at hand and apply the appropriate deep learning algorithms to accurately quantify the uncertainties (Rolf et al, 2024).

In this paper, we comprehensively review the uncertainty quantification approaches that have been applied within deep learning frameworks to address problems related to ECVs. In Section 2, we start by introducing the sources of uncertainties from a theoretical perspective and combine them with general processing pipelines of satellite observations to outline the nature of the problem. Then, we discuss the different perspectives from conventional statistics and deep learning. The bridge between the two perspectives is built based on analyzing the similarities and differences between them. Section 3 provides a review of deep learning uncertainty quantification approaches with a focus on those that have been applied in estimating ECVs. Section 4 presents two use cases by applying various deep learning algorithms to estimate two selected ECVs: snow cover fraction (SCF) and terrestrial water storage (TWS), discussing the different characteristics of derived uncertainties. Finally, we summarize our discussions and provide an outlook in Section 5.

2 ECV from Satellite Observations and Their Uncertainties

2.1 Overview of ECVs from Satellite Observations

GCOS currently specifies 55 ECVs, which are separated into three main domains: terrestrial, ocean, and atmosphere, and further sub-categorized into ten subdomains. In all the domains, satellite observations play a crucial role by providing global coverage of targeted variables with consistent quality, resulting in substantial contributions to determining ECVs. Previous studies have reported that satellite Earth observation data contribute to 33 ECVs significantly (Miranda Espinosa et al, 2020) and 42 ECVs at least partially (Giuliani et al, 2020; Ballari et al, 2023). Recent developments have increased this number to 51 out of 55 ECVs, which are at least partially estimated from sEO data. Space agencies worldwide have supported ambitious programs to develop measurement approaches, algorithms for retrieving ECVs from satellite observations, output products that document ECVs, and maintain continuous services to the community. Some exemplary platforms are provided by the European governments, including the Copernicus Climate Change Service (C3S; Buontempo et al 2022); the ESA Climate Change Initiative (ESA CCI; Plummer et al 2017); the Copernicus Land Monitoring Service (CLMS); EUMETSAT, and the US government, including the Physical Oceanography Distributed Active Archive Center (PODAAC), the National Oceanic and Atmospheric Administration (NOAA), and the NASA MEaSUREs program. These services have made ECV products more easily accessible globally to the broader community and have helped document progress toward global sustainable development targets (Anderson et al, 2017), improve the quality of reanalysis products, improve climate models through data assimilation approaches, and also help support critical decisions and policies related to the management of our resources, e.g. groundwater resources (Springer et al, 2023; Tapley et al, 2019).

The geosciences and climate scientists have widely realized the potential of deep learning algorithms, which can be applied to most, if not all, of the ECVs. A summary of these studies is given in Table 1. A common idea is to derive the relationship between sEO-based ECVs and in-situ measurements using deep learning algorithms to improve the accuracy and spatio-temporal resolutions of the sEO-based ECV products (e.g., Yang et al, 2021; Kolluru and Tiwari, 2022; Koppa et al, 2022; Cui et al, 2023; Chen et al, 2024). We can also benefit from this strategy to build empirical relationships between ECVs that are not directly observable from satellite measurements and other sEO-derived quantities to enable a quasi-sEO estimation (Hamrani et al, 2020). Clarifying the possible uncertainty sources in sEO data processing pipelines and linking them to the deep learning uncertainty quantification approaches is crucial for delivering realistic uncertainty information. Moreover, most of the applications of deep learning to ECV estimations deal with regression problems (i.e., providing continuous numerical value) with some exceptions, such as land cover classification (Jagannathan and Divya, 2021) or fire detection (Sathishkumar et al, 2023) requiring classification or segmentation (also known as pixel-wise classification). Given this trend, we will focus

on uncertainty quantification approaches for regression problems using deep learning techniques and try to bridge them with the classical statistical methods in the remainder of this paper.

2.2 Different uncertainties within satellite-based estimating pipeline

2.2.1 Definition of uncertainties and their coupled nature

Uncertainties can be categorized into *aleatoric uncertainty* (data uncertainty) and *epistemic uncertainty* (model uncertainty). Aleatoric uncertainty is caused by the inherent randomness of an event, such as uncertainties contained in forcing data or unavoidable measurement errors. Therefore, this type of uncertainty is considered irreducible. On the contrary, epistemic uncertainty is caused by deficiencies in the model, also known as lack of knowledge. We note that the reasons for model deficiencies in a conventional statistical model can be fundamentally different from the ones for a deep learning model, which will be discussed later in Section 2.3. Here we try to clarify the source of aleatoric and epistemic uncertainties in a deep learning model based on the law of total variance. In a deep learning model, the trainable parameters $\boldsymbol{\theta}$ are usually estimated based on a given training dataset $\mathcal{D} = \{\mathbf{X}, \mathbf{Y}\}$. The inputs $\mathbf{X} = [\mathbf{x}_1, \dots, \mathbf{x}_n]^T \in \mathbb{R}^{n \times d}$ contains n vectors with d features, whereas the targets $\mathbf{Y} = [y_1, \dots, y_n]^T \in \mathbb{R}^{n \times 1}$ contains n values (may also generalize to multi-dimensional vectors, see, e.g., Goodfellow et al, 2016). Once we apply this model to a new and unseen input \mathbf{x}^* (inference), we can obtain the corresponding prediction y^* with the associated total variance as:

$$\text{Var}(y^*|\mathbf{x}^*) = \underbrace{\mathbb{E}_{\boldsymbol{\theta}} [\text{Var}_{y^*}(y^*|\mathbf{x}^*, \boldsymbol{\theta})]}_{\text{Aleatoric}} + \underbrace{\text{Var}_{\boldsymbol{\theta}} (\mathbb{E}_{y^*} [y^*|\mathbf{x}^*, \boldsymbol{\theta}])}_{\text{Epistemic}}, \quad (1)$$

where the first term $\mathbb{E}_{\boldsymbol{\theta}}[*]$ describes the variability of the prediction y^* averaged over all the possible model parameters, quantifying the uncertainties caused by the inherent randomness of data regardless of the model parameters. Hence, it provides a rigorous definition of aleatoric uncertainties. The second term $\text{Var}_{\boldsymbol{\theta}}(*)$ measures the uncertainties of the mean of y^* given each model realization $\boldsymbol{\theta}$. By computing the expectation of all possible y^* , the inherent data randomness is averaged out, and therefore, the second term is understood as epistemic uncertainty (Krause, 2022). However, we should note that the definition given in Eq. (1) refers to uncertainty categories during inference based on the parameters $\boldsymbol{\theta}$ following the distribution of $p(\boldsymbol{\theta}|\mathcal{D})$ with the given training dataset \mathcal{D} . The defined epistemic uncertainty depends on the data (aleatoric) uncertainty of the training dataset (both inputs and targets), revealing the mixed nature of aleatoric and epistemic uncertainties. It has been argued that the aleatoric and epistemic uncertainties cannot be unambiguously separated (Hora, 1996), in particular for real-world data (Kahl et al, 2024). Recently, Gruber et al (2023) have given a comprehensive overview of the source of uncertainties in machine learning from a statistical view and confirmed this issue. With these thoughts, we clarify the definition of aleatoric and epistemic uncertainties used in this paper as follows:

Table 1: Overview of ECVs. The possible contributions from satellite observations and types of deep learning methods are listed. The ECVs that cannot be directly observed from satellite missions are marked in grey. The potential machine learning algorithms are categorized into regression (R) and classification (C). We note that the regression and classification tasks in this table also include grid-wise regression and classification, which are usually understood as segmentation tasks. Special notions: * denotes the studies with uncertainty quantification approaches; † denotes the studies without using sEO data.

Domain	Subdomain	Variables	Type of tasks	References	Exemplary data provision	
Terrestrial	Hydrosphere	Groundwater	R	Miro and Famiglietti (2018)	C3S	
		Lakes	R & C	Mullen et al (2023)	C3S	
		River discharge	R	Ansari et al (2023) [†]	ESA CCI	
		Soil moisture	R & C	Singh and Gaurav (2023)*	C3S	
		Evaporation from land	R	Koppa et al (2022)	OpenET	
			Terrestrial water storage	R	Gou and Soja (2024)*	C3S
	Cryosphere	Glaciers	R & C	Thomas et al (2023)	C3S	
		Ice sheets and ice shelves	R & C	Tollenaar et al (2024)*	C3S	
		Permafrost	R	Chen et al (2024)	ESA CCI	
		Snow	R & C	Cui et al (2023)	CLMS	
	Biosphere	Above-ground biomass	R	Zhang et al (2019)	ESA CCI	
		Albedo	R	Chen et al (2023)	C3S	
		Fire	R & C	Sathishkumar et al (2023) [†]	ESA CCI	
		FAPAR ¹	R	Ma et al (2022)	ESA CCI	
		Land cover	C	Jagannathan and Divya (2021)	CLMS	
		Land surface temperature	R	Wang et al (2021)	CLMS	
		Leaf area index	R	Castro-Valdecantos et al (2022)	ESA CCI	
		Soil carbon	R	Yang et al (2021)	-	
	Anthroposphere	Anthropogenic Greenhouse gas fluxes	R	Hamrani et al (2020)	-	
Anthropogenic water use		R	Wunsch et al (2022)* [†]	-		
Ocean	Physical	Ocean surface heat flux	R	George et al (2021)	NOAA	
		Sea ice	R & C	Andersson et al (2021)*	C3S	
		Sea level	R	Nieves et al (2021)*	C3S	
		Sea state	R	Mittendorf et al (2022) [†]	CMS	
		Sea surface currents	R	Sinha and Abernathy (2021) [†]	CMS	
		Sea surface salinity	R	Guillou et al (2023) [†]	CMS	
		Sea surface stress	R	Yousefi et al (2024) [†]	-	
		Sea surface temperature	R	Xiao et al (2019)*	C3S	
		Subsurface currents	R	Bradbury and Conley (2021) [†]	CMS	
		Subsurface salinity	R	Tian et al (2022)*	CMS	
			Subsurface temperature	R	Su et al (2022)	CMS
	Biogeochemical	Inorganic carbon	R	Galdies and Guerra (2023)	CMS	
		Nitrous oxide	R	Yang et al (2020)* [†]	CMS	
		Nutrients	R	Contractor and Roughan (2021)* [†]	CMS	
		Ocean colour	S	Kolluru and Tiwari (2022)	C3S	
		Oxygen	R	Sharp et al (2023)* [†]	CMS	
			Transient tracers	R	-	-
	Biological/ecosystems	Marine habitats	R & C	Rubbens et al (2023)	-	
		Plankton	R	Ciranni et al (2024) [†]	CMS	
Atmosphere	Surface	Precipitation	R	Gavahi et al (2023)	C3S	
		Pressure	R	Karmakar et al (2023) [†]	-	
		Radiation budget	R	Li et al (2022b)	C3S	
		Temperature	R	Shen et al (2020)	EUMETSAT	
		Water vapour	R	Wu et al (2023)	C3S	
			Wind speed and direction	R	Jiang et al (2024b) [†]	EUMETSAT
	Upper-air	Earth radiation budget	R	Yao et al (2023) [†]	C3S	
		Lightning	R	Zhou et al (2020)*	NASA	
		Temperature	R	Haynes et al (2024)*	EUMETSAT	
		Water vapour	R	Zhang et al (2024)	NASA	
		Wind speed and direction	R	Das et al (2021) [†]	EUMETSAT	
		Clouds	R & C	Wright et al (2024)*	C3S	
	Atmospheric Composition	Aerosols	R	Tao et al (2023)	ESA CCI	
Greenhouse gases		R	Altikat (2021) [†]	-		
Ozone		R	Han et al (2023)	-		
Precursors for aerosols and ozone		R	Tao et al (2024)	-		

- **Aleatoric uncertainties:** Uncertainties caused by data problems, including training and inference data. This category includes irreducible uncertainty due to inherent noise in the observational systems and outliers caused by problematic measurements or observing environments. Thus, we can confidently refer to them as data uncertainties.
- **Epistemic uncertainties:** Uncertainties caused by the imperfect model. The possible reasons include inadequate assumptions, difficulties in optimization (local optimum), inadequate training (under- or over-fitting), insufficient model capacity, etc.

Although the aleatoric and epistemic uncertainties cannot be precisely separated, the total uncertainties are defined in Eq. (1) with values independent of different categorizing strategies. Therefore, our ultimate goal is to quantify the total uncertainties as realistically as possible without overemphasizing the distinction between different types of uncertainties. As a matter of fact, the total uncertainties are the most crucial information for decision-makers.

2.2.2 Data processing pipeline and sources of uncertainties

To better understand the sources of uncertainties in a typical sEO-based ECV processing pipeline, we briefly describe the multiple levels of products and their associated uncertainty propagation (Povey and Grainger, 2015b; Mittaz et al, 2019). Fig. 1 depicts a typical estimating pipeline with both data (right side) and uncertainty (left side) propagation. From the raw observations to user-friendly products, the satellite data are processed through multiple levels, from Level-0 (L0, indicating raw measurements) to Level-1 (processed products with telemetry), Level-2 (geocoded, calibrated products), Level-3 (gridded products over the large scale) and finally Level-4 (L4, indicating highly processed products for specific targets) using a set of algorithms documented in Algorithm Theoretical Basis Documents (ATBDs). For each individual processing step, varying uncertainty sources may be involved, as shown in Fig. 1. The primary uncertainty resources for L0 data are the real-world variability and the inherent sensor noises. The L0 data uncertainty is the primary aleatoric source for L1 products with additional contribution with other auxiliary data uncertainties, whereas the used calibration models and processing strategies introduce epistemic uncertainties. All of these uncertainties are then together propagated to L1 products and become the aleatoric uncertainties in the L1 to L2 process. At this stage, more models are involved, such as background models or predefined geophysical relationships, causing increasing impacts of epistemic uncertainties. The processing steps from L2 onward usually involve multiple data and models for processing and corrections. Therefore, it is hard to judge if aleatoric or epistemic sources dominate the total uncertainties. It is undoubtedly necessary to rigorously consider all the uncertainty sources for a realistic final uncertainty quantification. The uncertainties in individual processing steps accumulate and propagate to the final L3 or L4 products for the users to make decisions. We should note that the practical processing levels of different satellite missions may slightly differ from each other. For example, the L1 steps is sometime further separated into L1a and

L1b steps and not all the generated products are available to the users. An example case is the GRACE(-FO) mission which is described in Appendix A.

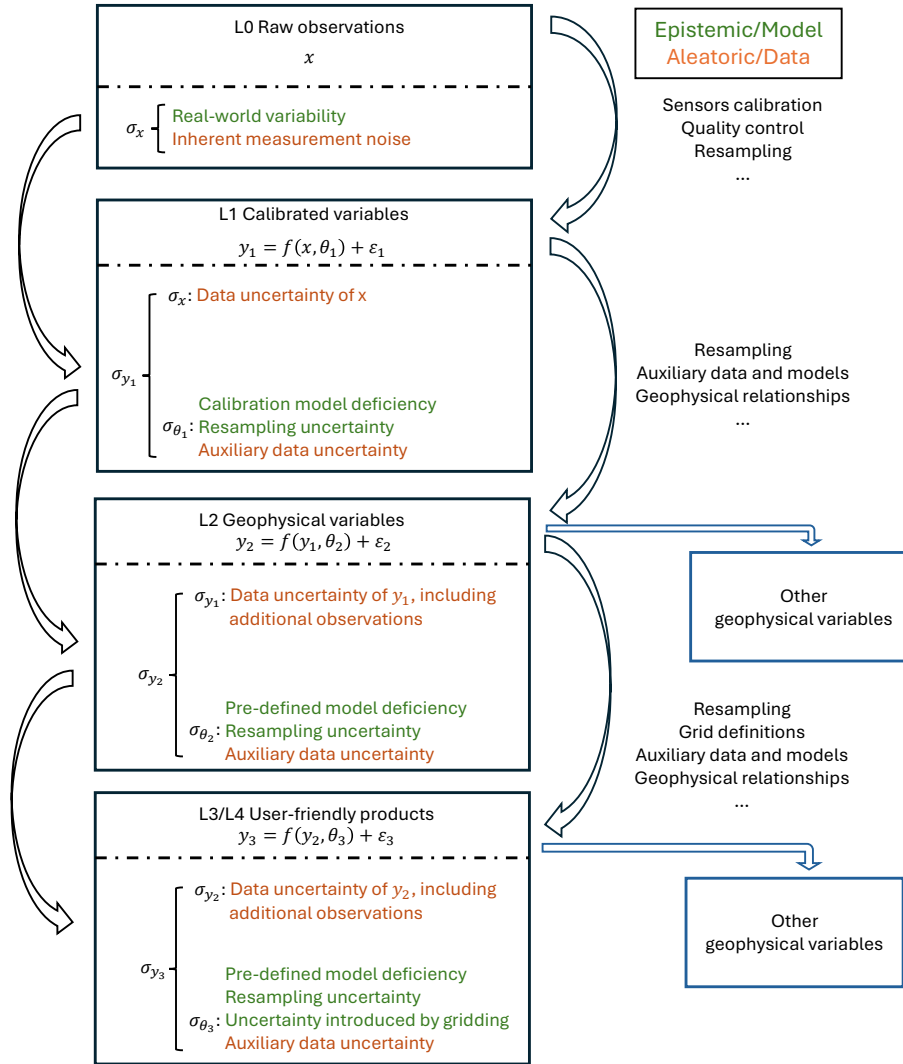


Fig. 1: Estimating pipeline of sEO-based variables from L0 to L4 and the corresponding uncertainty propagation. The uncertainties from models (epistemic) are denoted in green, whereas those from data (aleatoric) are denoted in orange. The right arrows denote the processing steps with necessary actions or additional information, whereas the left arrows indicate uncertainty propagation. The deep learning algorithms are usually applied to L2 to L4 products to derive other geophysical variables depicted in blue.

Furthermore, we highlight that different satellite-based ECVs rely on varying measuring principles, and therefore, the dominating sources of data uncertainties may be different. For example, ECVs based on imaging, namely the classical remote sensing at all the different wavelengths of interest, are dominated by the sensitivity and resolution of the equipped sensors as well as the observing environments (real-world variability), such as cloudy days (Toth and Józków, 2016). On the contrary, for ECVs that rely on geometry (e.g., satellite altimetry) orbit accuracy, especially in the radial direction, is of critical importance (Abdalla et al, 2021). For ECVs based on satellite gravimetry, the requirements for accuracies of multiple sensors further increase, including the inter-satellite ranging system and accelerometers for removing non-gravitational forces (Landerer et al, 2020). The situation is similar to the potential epistemic uncertainty sources. Varying models or predefined relationships based on domain expertise exist at the level of the algorithms used to retrieve ECVs from the sEO measurements. For instance, several ECVs are deduced from the reflectance or emission of electromagnetic waves from the ocean or land surface or atmospheric layers via (more primitive) regression analysis or (more advanced) semi-empirical, physically-based retrievals, such as chlorophyll concentration from ocean color (Elachi and Van Zyl, 2021; Martin, 2014). There may also be inherent limitations associated with these retrieval, for instance, uncertainties associated with the depth of the water column leading to sea surface temperature or the depth of soil layers leading to the retrieval of soil moisture. For the ECVs derived from signals that are tightly coupled with other geophysical signals (e.g., satellite gravimetry), the background model to isolate the signals of interest is critical (Shihora et al, 2022). We further provide a detailed example in Appendix A based on the whole processing pipeline of the GRACE(-FO) satellite data to clarify the complex sources of uncertainty. The exemplary pipeline again emphasizes the mixing nature of aleatoric and epistemic uncertainty. It may not be so critical to distinguish between them explicitly, but carefully considering the uncertainties in all steps is the key to reaching realistic product uncertainties and making optimal decisions.

2.3 Conventional statistical and deep learning views on uncertainty quantification

This section will clarify the sources of uncertainty from conventional statistical and deep learning points of view based on theoretical considerations. A least-square estimation model and a deep learning regression model share many common settings but also have different views, which cause different sources of uncertainties and ways to quantify them. To better highlight the differences between these two views, we need to clarify a fundamental difference in estimating parameters in a conventional statistical approach and a deep learning framework. Fig. 2 shows basic settings of a conventional least-square estimation and a deep learning regression problem for the training (or parameter estimation) process (see Butt et al, 2021; Kutz, 2023; Amiri-Simkooei et al, 2024, for further discussion).

In a typical least-square estimation, we are interested in determining a set of variables (denoted by $\beta \in \mathbb{R}^{m \times 1}$, where m denotes the number of parameters) that are usually not directly measurable or their direct measurements cannot reach the expected accuracy, but can be linked to a set of other observable data based on a

known (physics-based or empirical) relationship. It implies that in a least-square estimation, we typically solve an inverse problem by formulating the target variables as unknown parameters β in a predefined function $f(\mathbf{z}, \beta) = 0$ related to direct observations $\mathbf{z} \in \mathbb{R}^{n \times 1}$, where n indicates the number of samples. The function f may contain both the linearized relationship (parameterized by the design matrix \mathbf{A}) and conditional constraints (parameterized by the constraint matrix \mathbf{B}). By minimizing the root mean square residuals of the predefined function, we can find the optimal estimation of target variables and obtain their uncertainties based on the law of uncertainty propagation (Koch, 2013). In this aspect, the resulting uncertainties arise from input data uncertainties (aleatoric) under the given relationship f . The impacts of the model deficiency (epistemic uncertainty), usually known as the “+0” term, are unavoidably present but usually assumed to be small since the predefined function is assumed to be satisfactory accurate (Mittaz et al, 2019).

In a deep learning regression model, the functional relationship is typically unknown. Instead, the input-target pairs for the training set $\mathcal{D} = \{\mathbf{X}, \mathbf{Y}\}$ are available. We choose a deep learning model with a set of trainable parameters θ and estimate the relationship by minimizing the differences between predicted values $\hat{\mathbf{Y}}$ and labels \mathbf{Y} . The obtained model will be later applied to an unseen input set \mathbf{X}^* to get the corresponding \mathbf{Y}^* as the final predictions. Most efforts are usually put into quantifying the epistemic uncertainties, namely the uncertainties caused by θ , but the uncertainties caused by data uncertainty of both training and test sets may be overlooked (Gruber et al, 2023). One of the plausible reasons is that the data uncertainty is usually inaccessible for common data types used in deep learning, such as RGB-images (Deng et al, 2009). Therefore, most of the related investigations focus on the uncertainties caused by different model architectures and optimization processes.

From Fig. 2, we can understand the similarities of the two approaches. Certain sets of known data are available for the training process, and some target parameters are to be estimated. The primary difference is whether or not a strong prior knowledge is considered. A least-square model converts the raw inputs into the rows of the design matrix \mathbf{A} based on a strong prior knowledge imposed by the functional relationship f , which is designed based on domain expertise. The construction of the design matrix can be understood as a feature engineering (Zheng and Casari, 2018) which is usually needed for a machine learning model but not highly required for a deep learning model. The recent developments in deep learning models tend to feed the raw data \mathbf{X} into the model and believes the vast model capacity can exploit the information contained in data. The different views are also reflected in the target (unknown) parameters. The model parameters β are tightly coupled with the predefined function f , whereas the trainable parameters θ are rarely constrained by prior knowledge, except for the operator mechanisms involved in the model architecture, such as the shift-invariant feature of a convolutional kernel.

The above discussion also reveals the different perspectives on uncertainty quantification and the fundamental differences in the sources of uncertainties. The epistemic uncertainty in a conventional statistical model mainly comes from the misspecification of the pre-defined model (the “+0” term) because the sum of unmodelled effects rarely follows a zero-mean Gaussian distribution in practice. In this case, the pre-defined

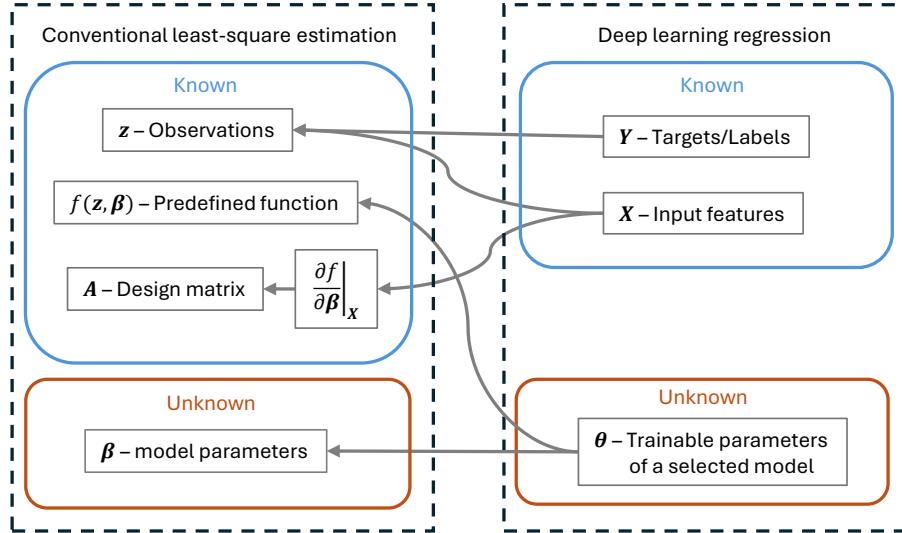


Fig. 2: A schematic comparison of a conventional least-square estimation model and a deep learning regression model for the training (or parameter estimation) process. The observations in a least-square estimation problem include both inputs and targets in a deep learning model. The unknown parameters and predefined function in a classical least-square estimation model are represented by a set of unknown but trainable parameters θ of a selected deep learning model.

relationship lacks knowledge of relevant effects because the necessary parameters to quantify them are not provided. So, the model cannot capture all the important effects or patterns in the data to reach the “best” estimation. This phenomenon can be understood as a typical underfitting issue since the conventional statistical model is typically low-dimensional (compared to deep learning) with high data redundancy. Section 2.3.1 will further clarify this issue with analytical expression. On the contrary, the model capacities of deep learning models are rarely a problem since they are typically massively over-parameterized. However, a huge number of trainable parameters and complicated model architectures may cause overfitting issues and high epistemic uncertainty. These issues require careful design of the deep learning model and can be eliminated by applying advanced optimizing strategies with careful diagnoses of the loss curves (Moradi et al, 2020; Tian and Zhang, 2022). Another rather dominating reason for epistemic uncertainty in a deep learning model is the incomplete (and thus biased) training data set. If the training data set is not fully representative and cannot cover the full data distribution, the obtained model may over-rely on the general pattern shown in the training set but does not exist in the test set and discard the possible patterns that are simply not covered by the training set. The origin of the epistemic uncertainty and the ways to quantify them with ECV application examples are introduced in Section 2.3.1 and Section 3, respectively.

Regarding the aleatoric uncertainty, the conventional statistical model can rigorously consider input uncertainty and also their covariances in the frame of uncertainty

propagation whenever we have a sample with associated uncertainty information. However, the uncertainty propagation approach is again highly dependent on the predefined relationship. Therefore, the aleatoric uncertainties are mixed with the epistemic uncertainties in this case (see Section 2.3.1). The deep learning techniques to quantify aleatoric uncertainty are rather limited compared to the ways to quantify epistemic uncertainty. The logic is to let the model "judge" its prediction by predicting the associated uncertainty together and formulate them in a different loss term (Kendall and Gal, 2017). An obvious limitation, especially for applications in satellite-based ECV studies, is the absence of treatment of input feature uncertainties, see Section 2.3.2, and Section 3.5.

2.3.1 Conventional statistical view

The most common uncertainty quantification approach incorporated in the processing pipelines for satellite-based ECVs is based on the frequentist approach, which is grounded in long-run frequencies and relies heavily on techniques such as confidence intervals and hypothesis testing (Lehmann and Romano, 2005; Teunissen, 2006). While confidence intervals offer a range of values within which the true parameter is expected to lie with a specified probability (Efron, 1979), hypothesis testing involves making decisions about the validity of specific hypotheses based on sample data (Neyman and Pearson, 1933). Building upon these fundamentals, one widely used method in the frequentist approach for uncertainty quantification is to rely on maximum likelihood estimation (MLE). MLE seeks to find the parameter values that maximize the likelihood function, which measures the probability of the observed data given a set of parameters. The method provides estimates with desirable properties such as consistency, efficiency, and asymptotic normality (Casella et al, 2002). Considering a linear relationship and assuming the variables follow Gaussian distributions, MLE is equivalent to the least squares method, which is one of the most favorable approaches for uncertainty quantification within the frequentist framework. In this context, uncertainty quantification is typically performed by deriving a covariance matrix for the unknown parameters. To illustrate this, consider the Gauss-Helmert model (Teunissen, 2024), which is a combination of the Gauss-Markov model (A-model) and the conditional adjustment (B-model), see Koch (2013) for further discussion. In such a mixed model with both target parameter vectors $\boldsymbol{\beta}$ and observation vectors \mathbf{z} with associated covariance matrix $D(\mathbf{z}) = \mathbf{Q}_z$ being involved, the model is typically written as:

$$f(\mathbf{z}, \boldsymbol{\beta}) \stackrel{!}{=} \mathbf{0}, \quad (2)$$

meaning that the target is to minimize the misfit residuals, which is achieved by minimizing mean-square errors in a classical least-squares approach.

Eq. (2) indicates that we have knowledge of the relationships between the observations and the target parameters and can also provide knowledge about constraints applied on target parameters themselves (conditional adjustment). In reality, Eq. 2 is rarely linear, so we establish Taylor points $(\boldsymbol{\beta}_0, \mathbf{z}_0)$ for both the unknowns $\boldsymbol{\beta}$ and

observations \mathbf{z} as:

$$\tilde{\boldsymbol{\beta}} = \boldsymbol{\beta}_0 + \Delta\boldsymbol{\beta}, \quad (3)$$

$$\tilde{\mathbf{z}} = \mathbf{z} + \mathbf{e} = \mathbf{z} - \mathbf{z}_0 + \mathbf{z}_0 + \mathbf{e} = \mathbf{z}_0 + \Delta\mathbf{z} + \mathbf{e}, \quad (4)$$

with \mathbf{e} denoting the misfit residuals, so that the model can be linearized as:

$$\begin{aligned} f(\tilde{\mathbf{z}}, \tilde{\boldsymbol{\beta}}) &= f(\mathbf{z}_0 + \Delta\mathbf{z} + \mathbf{e}, \boldsymbol{\beta}_0 + \Delta\boldsymbol{\beta}) \\ &= \underbrace{f(\mathbf{z}, \boldsymbol{\beta})|_0}_{\mathbf{w}_0} + \underbrace{\frac{\partial f(\mathbf{z}, \boldsymbol{\beta})}{\partial \mathbf{z}}|_0}_{\mathbf{B}^T} (\Delta\mathbf{z} + \mathbf{e}) + \underbrace{\frac{\partial f(\mathbf{z}, \boldsymbol{\beta})}{\partial \boldsymbol{\beta}}|_0}_{\mathbf{A}} \Delta\boldsymbol{\beta} \end{aligned} \quad (5)$$

$$= \underbrace{\mathbf{w}_0 + \mathbf{B}^T \Delta\mathbf{z}}_{\mathbf{w}} + \mathbf{B}^T \mathbf{e} + \mathbf{A} \Delta\boldsymbol{\beta} \quad (6)$$

$$= \mathbf{w} + \mathbf{B}^T \mathbf{e} + \mathbf{A} \Delta\boldsymbol{\beta} \stackrel{!}{=} \mathbf{0}. \quad (7)$$

With such a formulation the cost function Eq. (7) is $\mathbf{e}^T \mathbf{P} \mathbf{e}$ with \mathbf{P} being the weight matrix for observations, defined as $\mathbf{P} = \sigma_0^2 \mathbf{Q}_z^{-1}$. The solutions take the forms:

$$\Delta\hat{\boldsymbol{\beta}} = -[\mathbf{A}^T (\mathbf{B}^T \mathbf{P}^{-1} \mathbf{B})^{-1} \mathbf{A}]^{-1} \mathbf{A}^T (\mathbf{B}^T \mathbf{P}^{-1} \mathbf{B})^{-1} \mathbf{w}, \quad (8)$$

$$\hat{\mathbf{e}} = -\mathbf{B} \mathbf{P}^{-1} (\mathbf{B}^T \mathbf{P}^{-1} \mathbf{B})^{-1} (\mathbf{w} + \mathbf{A} \Delta\hat{\boldsymbol{\beta}}), \quad (9)$$

with a-posteriori estimate of σ_0^2 as

$$\hat{\sigma}_0^2 = \frac{\hat{\mathbf{e}}^T \mathbf{P} \hat{\mathbf{e}}}{\text{d.o.f.}}, \quad (10)$$

with d.o.f. stands for degree of freedom. The uncertainty of the estimated parameters $\hat{\boldsymbol{\beta}}$ is then quantified based on uncertainty propagation law:

$$\hat{\mathbf{Q}}_{\hat{\boldsymbol{\beta}}} = \hat{\sigma}_0^2 (\mathbf{A}^T (\mathbf{B}^T \mathbf{P}^{-1} \mathbf{B})^{-1} \mathbf{A})^{-1}. \quad (11)$$

Therefore, the estimated uncertainty of $\hat{\boldsymbol{\beta}}$ depends on the observation uncertainties \mathbf{Q}_z , the predefined functional relationship (Eq. 2) and also its Taylor expansion (Eq. 5). The first term is the aleatoric part of the total uncertainty and rigorously considered in a least-square estimation. The last two factors together form the epistemic part of the total uncertainty, although their impacts are usually argued to be small by assuming the pre-defined relationship Eq. (2) is accurate and all the "+0" term to be zero-mean Gaussian. It is clear that the aleatoric and epistemic uncertainties are coupled in the uncertainty propagation approach.

2.3.2 Deep learning view

To show the uncertainty sources in a deep learning regression model, we start the discussion with a relatively simple case. Following the definitions in the previous sections,

$\mathbf{X} = [\mathbf{x}_1, \dots, \mathbf{x}_n]^T$ denote the input dataset, and $\mathbf{Y} = [\mathbf{y}_1, \dots, \mathbf{y}_n]^T$ denote the corresponding target dataset. The pair $\mathcal{D} = \{\mathbf{X}, \mathbf{Y}\}$ denotes the training dataset of n samples. Considering a linear relationship constrained by the regularization parameter λ (Khalaf and Shukur 2005, so-called Ridge regression or L2-regularization), we can find the analytical solution:

$$\hat{\boldsymbol{\theta}} = (\mathbf{X}^T \mathbf{X} + \lambda \mathbf{I})^{-1} \mathbf{X}^T \mathbf{Y}, \quad (12)$$

which is equivalent to finding the mode of the full posterior distributions (Deisenroth et al, 2020):

$$\arg \min_{\boldsymbol{\theta}} \sum_{i=1}^n (y_i - \boldsymbol{\theta}^T \mathbf{x}_i)^2 + \lambda \|\boldsymbol{\theta}\|_2^2 \equiv \arg \max_{\boldsymbol{\theta}} P(\boldsymbol{\theta}) \prod_i P(y_i | \mathbf{x}_i, \boldsymbol{\theta}). \quad (13)$$

Assuming the prior distributions of parameters are independent Gaussian distributions $p(\boldsymbol{\theta}) = \mathcal{N}(0, \sigma_p \mathbf{I})$, and the likelihood are conditionally independent $p(y_i | \boldsymbol{\theta}, x_i) = \prod_i P(y_i | \mathbf{x}_i, \boldsymbol{\theta}) = \prod_i \mathcal{N}(y_i; \boldsymbol{\theta}^T \mathbf{x}_i, \sigma_n^2)$, the inference given a new set of inputs \mathbf{x}^* can be analytically expressed as:

$$p(y^* | \mathbf{x}^*, \hat{\boldsymbol{\theta}}) = \mathcal{N}(y^*; \hat{\boldsymbol{\theta}}^T \mathbf{x}^*, \sigma_n^2), \quad (14)$$

indicating that y^* is sampled from a Gaussian distribution with the expectation of $\hat{\boldsymbol{\theta}}^T \mathbf{x}^*$ and variance of σ_n^2 . The most plausible mode estimation of $f^* = \hat{\boldsymbol{\theta}}^T \mathbf{x}^*$ is associated with inherent random noise σ_n (aleatoric uncertainty). Since the prediction of a Ridge regression focuses on the mode rather than providing the full posterior distribution, it provides no information on the epistemic uncertainty.

To consider the distribution of trainable parameters $\boldsymbol{\theta}$ based on Bayesian statistics, we estimate the whole posterior distributions $p(\boldsymbol{\theta} | \mathcal{D})$ instead of the mode $\hat{\boldsymbol{\theta}}$. The posterior distribution of the trainable parameters $\boldsymbol{\theta}$ can be expressed using Bayes' theorem:

$$p(\boldsymbol{\theta} | \mathcal{D}) = \frac{p(\mathcal{D} | \boldsymbol{\theta}) p(\boldsymbol{\theta})}{p(\mathcal{D})}. \quad (15)$$

In this way, we generalize the ridge regression to Bayesian linear regression (BLR) and also consider the discrepancies among different parameters given the same set of training samples (epistemic uncertainties). It is worth noting that a BLR model is nothing else but a Gaussian process regression (the same as the well-known Kriging or Collocation in the geoscience community) with a linear kernel (Deisenroth et al, 2020). By inference, the predictive distribution of \mathbf{y}^* is given by:

$$p(y^* | \mathbf{x}^*, \boldsymbol{\theta}) = \int p(y^* | \mathbf{x}^*, \boldsymbol{\theta}) p(\boldsymbol{\theta} | \mathcal{D}) d\boldsymbol{\theta} = \mathcal{N}\left(\hat{\boldsymbol{\theta}}^T \mathbf{x}^*, \mathbf{x}^{*T} \Sigma \mathbf{x}^* + \sigma_n^2\right), \quad (16)$$

from which we can obtain the uncertainties associated with the model and data. The first part, $p(y^* | \mathbf{x}^*, \boldsymbol{\theta})$, describes the prediction, given the input data and the model, whereas the second part, $p(\boldsymbol{\theta} | \mathcal{D})$, describes the model distribution, given the data. The

variances of different possible parameters, i.e., the epistemic uncertainty, is described by $\Sigma = (\mathbf{X}^T \mathbf{X} + \sigma_n^{-2} \mathbf{I})^{-1}$. At this stage, it is evident that this epistemic uncertainty is coupled with input data and the associated uncertainty (aleatoric) and, therefore, challenging to be fully separated.

So far, we have attempted to clarify the sources of both aleatoric and epistemic uncertainties in a BLR model. However, we have made three strong, and practically uncommon assumptions: (i) The input-target relationship is linear; (ii) All the relevant distributions are Gaussian; (iii) The aleatoric uncertainties are homoscedastic, namely independent of inputs. We briefly introduce the solutions for reducing these three assumptions in the following parts of this section, followed by a detailed discussion and literature review in Section 3.

To tackle the first issue, we move from BLR to Bayesian deep learning (BDL)², in which the linear regression is replaced by a neural network (LeCun et al, 2015; Goodfellow et al, 2016):

$$f(\mathbf{x}; \boldsymbol{\theta}) = \varphi_L(\varphi_{L-1}(\cdots \varphi_1(\mathbf{x}))), \quad (17)$$

where φ_L denotes the projection of the L^{th} layer which is typically composed of trainable parameters $\boldsymbol{\theta}_L$ (weights and biases) and non-linear activation functions. It is worth noting that the prior distributions of $\boldsymbol{\theta}_L$ are typically assumed as isotropic Gaussian distributions without credible prior information (Fortuin et al, 2021), meaning that the derived posterior distribution may not strictly follow the full Bayesian statistics. Therefore, the whole approach may be better understood as a pragmatic, Bayesian-inspired computation. In principle, such a neural network can approximate any non-linear relationship accurately (Hornik et al, 1989), but the computational complexity will increase remarkably.

By generalizing from Gaussian distribution to all possible distributions (second issue), a crucial problem arises that the posterior distribution $p(\boldsymbol{\theta}|\mathcal{D})$ cannot be computed analytically, and therefore, the second equal sign in Eq (16) does not hold anymore. This issue brings the challenge of determining the epistemic uncertainty associated with such neural networks. To this end, we need to approximate the complicated distributions by simpler distributions, which is known as variational approximation (Blei et al, 2017). A huge amount of effort has been dedicated to solving this issue to obtain realistic epistemic uncertainties by considering different requirements (Abdar et al, 2021; Gawlikowski et al, 2023), which we will discuss in detail focusing on the ones have been applied to ECV studies (Section 3).

Finally, the aleatoric uncertainties usually depend on the corresponding input data uncertainties, as discussed in Section 2.3.1. To this end, the heteroscedastic aleatoric uncertainties (issue 3) are crucial for ECVs, given the varying quality of input data. In a typical BDL pipeline, the heteroscedastic aleatoric uncertainties can be estimated by adding an output of the dedicated neural network to represent the associated variance

²Some debate exists about whether BDL algorithms are fully Bayesian or just probabilistic. We use the term BDL without implying the former, to remain consistent with existing literature.

of the predictions (Kendall and Gal, 2017):

$$p(\mathbf{y}^*|\mathbf{x}^*, \mathcal{D}) \sim \mathcal{N}(\boldsymbol{\mu}(\mathbf{x}^*; \boldsymbol{\theta}_1), \boldsymbol{\sigma}_{\text{ale}}^2(\mathbf{x}^*; \boldsymbol{\theta}_2)), \quad (18)$$

$$\boldsymbol{\mu}(\mathbf{x}^*; \boldsymbol{\theta}_1) = f(\mathbf{x}^*; \boldsymbol{\theta}_1), \quad (19)$$

$$\boldsymbol{\sigma}_{\text{ale}}^2(\mathbf{x}^*; \boldsymbol{\theta}_2) = \exp(f(\mathbf{x}^*; \boldsymbol{\theta}_2)), \quad (20)$$

where $\boldsymbol{\mu}$ and $\boldsymbol{\sigma}_{\text{ale}}^2$ are the two outputs of the same neural network f but parameterized by different parameters $\boldsymbol{\theta}_1$ and $\boldsymbol{\theta}_2$. The differences may only be present in the output layer. The positive values of the estimated variances are ensured by $\exp(*)$, which can be replaced by other positive functions. By assuming a Gaussian likelihood, we formulate the negative log-likelihood loss function as:

$$\begin{aligned} \mathcal{L}(\boldsymbol{\theta}) &= -\log p_{\boldsymbol{\theta}}(\mathbf{Y}|\mathbf{X}, \boldsymbol{\theta}) \\ &= \frac{1}{2} \log(\boldsymbol{\sigma}_{\text{ale}}^2) + \frac{1}{2} (\mathbf{Y} - \boldsymbol{\mu})^T \text{diag}(\boldsymbol{\sigma}_{\text{ale}}^{-2}) (\mathbf{Y} - \boldsymbol{\mu}) + \text{constant}, \end{aligned} \quad (21)$$

but can also be derived based on other tractable distributions (Nair et al, 2022; Kiani Shahvandi et al, 2025). With this modification, the training input uncertainties are considered (although only implicitly), especially when the training dataset covers a reasonably large partition of the whole data distribution. However, certain limitations exist. First, the covariances cannot be estimated since the large number of parameters makes all but the sparsest covariance matrices intractable. Second, the implicit consideration of input uncertainties may result in unrealistic uncertainties of the outputs, and the associated uncertainty of \mathbf{x}^* during inference is hardly considered since the same input values may be associated with totally different uncertainties. This issue is critical for ECV studies when dealing with real-world sEO data. Some alternative ways to quantify the aleatoric uncertainties based on the available uncertainty information of inputs will be discussed in Section 3.5.

3 Uncertainty quantification in deep learning

3.1 Methods for solving the posterior distribution of parameters

As described in the previous section, the posterior model distribution $p(\boldsymbol{\theta}|\mathcal{D})$ cannot be expressed analytically without linear relationship and Gaussian assumptions. The preliminary task in Bayesian deep learning is to find a way to approximate the posterior distribution to the best possible extent. One of the most rigorous ways of this approximation task is to use a posterior distribution based on variational parameters with simpler distributions, such as Gaussian. This approach is known as variational inference (VI) and is widely used in the machine learning community (Blei et al, 2017). Due to computational complexity, various studies are dedicated to achieving similar performance without explicitly finding variational parameters (Wilson and Izmailov, 2020; Jospin et al, 2022). The categorizations of different BDL algorithms might vary slightly within existing literature (Abdar et al, 2021; Gawlikowski et al, 2023). We choose to categorize the different BDL methods into the following four classes and describe each in detail in the following subsections:

- **Bayesian neural network (BNN)** refers to neural networks with all parameters associated with distributions instead of only modes. These distributions can be explicitly approximated by gradient-based optimization or fitting locally based on tractable distributions like Gaussian. The detailed techniques and applications to ECVs are listed in Section 3.2.
- **Sampling methods** refer to the approaches that directly sample the output distributions but do not approximate the distributions of model parameters. Although the model parameters are still associated with certain distributions, they are not explicitly expressed. Section 3.3 introduces Monte Carlo sampling and also the special adaptations based on the characteristics of neural networks. These methods do not require retraining multiple individual deep learning models.
- **Ensemble methods** refer to the approaches that require training and aggregating multiple individual deterministic models. The distributions of model parameters are not explicitly estimated. However, the variance of the outputs can be quantified by considering the differences among different ensemble members. Some of the widely-used ensemble methods are introduced in Section 3.4.
- **Other methods** include additional methods with special modifications for specific goals, especially for modern developments towards large models with big data, see Section 3.6. They may have some overlap with the first three categories.

3.2 Bayesian neural networks

Contrary to classical deep learning neural networks, which estimate the modes of each trainable parameter during training, a BNN attempts to model the full posterior distribution $p(\boldsymbol{\theta}|\mathcal{D})$ of all trainable parameters $\boldsymbol{\theta}$ given a set of training data \mathcal{D} . As mentioned in Section 3.1, the posterior distribution $p(\boldsymbol{\theta}|\mathcal{D})$ cannot be computed analytically, especially for highly non-linear deep learning models and when the parameters have high dimensions. The idea is to approximate the posterior distribution by

some simpler and tractable distributions $q_{\lambda}(\boldsymbol{\theta})$ (called variational distributions), such as the Gaussian distribution, characterized by another set of parameters $\boldsymbol{\lambda}$. To achieve this goal, we try to maximize the similarity between the two distributions. In practice, we may minimize the Kullback-Leibler (KL) divergence (Kullback and Leibler, 1951) by adjusting $\boldsymbol{\lambda}$:

$$\text{KL}(q_{\lambda}(\boldsymbol{\theta})||p(\boldsymbol{\theta}|\mathcal{D})) = \int q_{\lambda}(\boldsymbol{\theta}) \log \frac{q_{\lambda}(\boldsymbol{\theta})}{p(\boldsymbol{\theta}|\mathcal{D})} d\boldsymbol{\theta}. \quad (22)$$

The KL divergence is a measure of how similar two probability distributions are, and is frequently used as a loss function for VI in machine learning. In the following subsections, we discuss how to adapt the KL divergence and incorporate it into the optimizing process of a neural network.

3.2.1 Bayes by Backprop

Bayes by Backprop (Blundell et al, 2015) is a famous adaption of VI to deep neural networks. To find the variational distribution that can minimize the KL divergence (Eq. (22)) under the constraint of given dataset \mathcal{D} , we can rearrange the optimization problem into evidence lower bound (ELBO) maximization:

$$\arg \min_{q \in Q} \text{KL}(q_{\lambda}||p(\boldsymbol{\theta}|\mathcal{D})) = \arg \max_{q \in Q} \underbrace{\{\mathbb{E}_{\boldsymbol{\theta} \sim q} [p(Y|\boldsymbol{\theta})] - \text{KL}(q_{\lambda}||p(\boldsymbol{\theta}))\}}_{\text{ELBO}, \mathcal{L}(q)}, \quad (23)$$

which saves us from solving the posterior distributions. If we consider the distribution family Q as Gaussian, we can formulate the targeted variational distributions as $q(\boldsymbol{\theta}|\boldsymbol{\lambda}) = \mathcal{N}(\boldsymbol{\theta}; \boldsymbol{\mu}, \boldsymbol{\Sigma})$, where $\boldsymbol{\lambda}$ indicates the trainable parameters that should be optimized during backpropagation. Instead of estimating $\boldsymbol{\theta}$ during training, we estimate $\boldsymbol{\mu}$ and $\boldsymbol{\Sigma}$ on \mathcal{D} . The mean vector and covariance matrix may be estimated using the re-parameterization trick (Kingma et al, 2015) that detaches the $\boldsymbol{\mu}$ and $\boldsymbol{\Sigma}$ from the randomness in the approximate posterior. Hence, we model the parameters via

$$\boldsymbol{\theta} = \boldsymbol{\mu} + \boldsymbol{\sigma} \odot \boldsymbol{\epsilon}, \quad (24)$$

where $\boldsymbol{\sigma}$ denotes the diagonal of $\boldsymbol{\Sigma}^{1/2}$ and $\boldsymbol{\epsilon} \sim \mathcal{N}(\mathbf{0}, \mathbf{I})$. Then, we can reformulate ELBO into a target loss function with respect to $\boldsymbol{\lambda}$ with the gradients as:

$$\nabla_{\boldsymbol{\lambda}} \mathcal{L}(\boldsymbol{\lambda}) = \nabla_{\boldsymbol{\sigma}, \boldsymbol{\mu}} \mathbb{E}_{\boldsymbol{\epsilon} \sim \mathcal{N}(\mathbf{0}, \mathbf{I})} [\log p(Y|\boldsymbol{\mu} + \boldsymbol{\sigma} \odot \boldsymbol{\epsilon})] - \nabla_{\boldsymbol{\sigma}, \boldsymbol{\mu}} \text{KL}(q_{\boldsymbol{\sigma}, \boldsymbol{\mu}}||p(\boldsymbol{\theta})), \quad (25)$$

which has an analytical solution. Therefore, we can find the optimal solution using classical optimization algorithms, such as Adam (Kingma and Ba, 2014). After training a BNN, we approximate the final posterior distribution $p(\mathbf{y}^*|\mathbf{x}^*, \mathcal{D})$ by using sampling methods, namely drawing M sets of weights from the weights distribution and make the final predictions:

$$p(y^*|\mathbf{x}^*, \mathcal{D}) = \mathbb{E}_{\boldsymbol{\theta} \sim q(\boldsymbol{\theta}|\boldsymbol{\lambda})} [p(\mathbf{y}^*|\mathbf{x}^*, \boldsymbol{\theta})] \quad (26)$$

$$\approx \frac{1}{M} \sum_{m=1}^M p\left(y^* | \mathbf{x}^*, \boldsymbol{\theta}^{(m)}\right). \quad (27)$$

3.2.2 Laplace approximation

In Laplace approximation (MacKay, 1992), we also approximate the posterior distribution $p(\boldsymbol{\theta}|\mathcal{D})$ using a Gaussian distribution around the true posterior using a second-order Taylor expansion around the posterior mode $\hat{\boldsymbol{\theta}}$:

$$\log p(\boldsymbol{\theta}|\mathcal{D}) \approx \log p(\hat{\boldsymbol{\theta}}|\mathcal{D}) + \frac{1}{2} \left(\boldsymbol{\theta} - \hat{\boldsymbol{\theta}}\right)^T \left(\mathbf{H} + \epsilon \mathbf{I}\right) \left(\boldsymbol{\theta} - \hat{\boldsymbol{\theta}}\right), \quad (28)$$

where \mathbf{H} is the Hessian matrix of $\log p(\boldsymbol{\theta}|\mathcal{D})$. The posterior distribution can be expressed as:

$$p(\boldsymbol{\theta}|\mathcal{D}) = \mathcal{N}\left(\hat{\boldsymbol{\theta}}, (\mathbf{H} + \epsilon \mathbf{I})^{-1}\right). \quad (29)$$

Inverting the Hessian matrix is computationally very heavy, and therefore the Laplacian approximation is often applied to the last layer of the network (Kristiadi et al, 2020).

3.2.3 Applying BNN to ECVs

The value of BNN has been widely realized due to its relatively solid theoretical background. Prior to the developments in approximating the posterior distributions using gradient-based optimization algorithms, the approximation of posterior distributions primarily relied upon methods such as Laplacian approximation. Khan and Coulibaly (2006) designed a BNN based on multilayer perceptron (MLP) to model the rainfall-runoff relationship with uncertainty quantification. Moreover, they highlighted that the BNN outperformed the conventional MLP model with less severe overfitting issues because of considering parameter uncertainties. Following studies applied similar strategies to model other ECVs including groundwater level (Maiti and Tiwari, 2014).

In recent years, Bayes by Backprop and its variants (see, e.g., Liu and Wang, 2016) have been gaining more attention since they can be efficiently solved by existing gradient-based optimization techniques. Moreover, such methods are easier to be generalized to large data volumes and fit the current direction of developments towards "big data" and foundation models (Li et al, 2023). Various studies employed this technique to estimate ECVs and achieved superior accuracies with realistic uncertainty information. Clare et al (2022) applied BNN to classify dynamical ocean regimes and connect their uncertainty analysis with explainable artificial intelligence (xAI) techniques to improve the trustworthiness of proposed models. Mo et al (2022) and Uz et al (2022) both employed Bayesian convolutional neural networks (BCNN) to bridge the one-year gap between GRACE and GRACE-FO missions to provide a continuous record of global TWS anomalies. The realistic predictive uncertainties are provided together with satisfactorily high-quality predictions. However, the trends reconstructed by BCNN are relatively less accurate than other methods such as deep convolutional auto encoders (Uz et al, 2022), indicating the issue that BNN may have

lower generalizability than other simpler proxies under domain shift (Izmailov et al, 2021). The short-term variability of the sea surface temperature was satisfactorily predicted by using BNN (Luo et al, 2022). With the quantified uncertainties inherent in the data and caused by model itself, reasonable risk assessment can be performed while using the temperature prediction for forecasting extreme events. Kang et al (2024) applied BNN to estimate the relationship between source zone metrics and mass discharge, outperforming the existing upscaled models with fewer parameters and providing uncertainty information. Such an uncertainty-aware model holds great potential for risk assessments and decision making. A similar model was employed by Xu et al (2021) for forecasting precipitation. They highlighted that the predictand data uncertainty might be ignored in a typical BNN pipeline and, therefore, proposed to jointly model the input/target data uncertainties and model uncertainties. This method is crucial towards a more realistic uncertainty quantification as we described in Section 2.3.2 and will be further discussed in Section 3.5. A common finding from all the mentioned studies is that the accuracy and computational costs of BNNs critically depend on the pre-defined prior distributions (Fortuin et al, 2021; Jospin et al, 2022), which need to be carefully designed in advance.

3.3 Sampling methods

Although approximating the full posterior distributions based on VI provides the most rigorous information on the distribution of parameters, certain limits exist, including the computational cost, optimization difficulty, and sensitivity to prior distributions. Alternatively, we can sample from the posterior distribution without explicitly estimating it using Monte Carlo simulation. By combining these principles with deep neural networks, unique opportunities are enabled that can be exploited for the purpose of uncertainty quantification.

3.3.1 Markov Chain Monte Carlo

Markov Chain Monte Carlo (MCMC, Neal 1992, 2011), is a powerful technique used in statistics and various other fields to sample from complex probability distributions. It allows us to "explore" these distributions by generating sets of random samples that "resemble" the true underlying distribution, regardless of the complexity of this distribution. The sampling techniques are practical for approximating the predictive distribution of possible neural network parameters since the integral of the predictive distribution is often intractable.

MCMC relies on Markov chains (Bishop, 2006), which are sequences of random values where each value depends only on the previous one. MCMC constructs a chain that "walks through the landscape" set out by the desired distribution. Each step involves proposing a new value based on the current one and accepting or rejecting it probabilistically. The "walk" continues until the chain reaches equilibrium, meaning the distribution of values visited resembles the target distribution. Keeping track of the accepted values after reaching equilibrium allows us to get samples that reflect the target distribution, even if we could not directly sample from it:

$$\boldsymbol{\theta}_t \sim q(\boldsymbol{\theta}_t | \boldsymbol{\theta}_{t-1}, \mathcal{D}). \quad (30)$$

The number of transitions needs to be performed T times, which must be determined in advance. Once we determine a sequence of weights $\boldsymbol{\theta}_1 \dots \boldsymbol{\theta}_T$, the prediction reads:

$$p(y^*|\mathbf{x}^*, \mathcal{D}) \approx \frac{1}{T} \sum_{t=1}^T p(y^*|\mathbf{x}^*, \boldsymbol{\theta}_t). \quad (31)$$

However, the optimal value of T is usually unknown and needs to be determined based on experiments. Moreover, the computational cost for MCMC is very high, especially for today’s modern deep neural networks. Even though MCMC is the gold standard for sampling from complex distributions, they are not tractable for deep learning networks with billions of parameters. The huge size of trainable parameters prohibits saving the full set of parameters in a Markov chain, whereas modern big datasets cannot be processed at once but require stochastic training strategies.

3.3.2 Monte Carlo dropout

Monte Carlo dropout (MC-Dropout; Gal and Ghahramani 2016) is a special application of Monte Carlo methods to deep neural networks based on the dropout mechanism (Srivastava et al, 2014). The dropout mechanism can be expressed as:

$$\boldsymbol{\theta}^{(i)} = \mathbf{s}^{(i)} \odot \boldsymbol{\theta}, \quad \mathbf{s}^{(i)} \sim \text{Bernoulli}(\mathbf{s}|\alpha), \quad (32)$$

where α denotes the probability that a node is activated and $\boldsymbol{\theta}$ denotes all trainable parameters in the model architecture. During each iteration, only this subset of the model parameters will be activated during the forward pass and optimized during backpropagation. Dropout is an efficient technique to mitigate the overfitting issue.

The principle of MC-Dropout is simple: we leverage the dropout also during inference, i.e., randomly selected nodes are deactivated to generate different outputs. The approach will be repeated T times, and the final output of the network is computed as Eq. (27). We can understand this approach as sampling from the full posterior distribution of $\boldsymbol{\theta}$ based on Eq. (32). Although we cannot explicitly express the distribution of $\boldsymbol{\theta}$, we can directly sample the final outputs from the marginal distribution, namely:

$$f(y^*|\mathbf{x}^*, \mathcal{D}) = \frac{1}{T} \sum_{t=1}^T \text{NN}_{\boldsymbol{\theta}^{(i)}}(\mathbf{x}^*), \quad (33)$$

where $\text{NN}_{\boldsymbol{\theta}^{(i)}}$ denotes the neural network with a subset parameters $\boldsymbol{\theta}^{(i)}$ activated.

A drawback of this approach is that the model architectures vary during inference (see also Section 3.4.2), so the possible parameter distributions are coupled with the possible model distributions, although both of them are understood as epistemic uncertainties. Additionally, employing dropout requires more careful hyperparameter tuning to avoid potential degradation of performance (Garbin et al, 2020).

3.3.3 Stochastic weight averaging

Stochastic weight averaging (SWA; Izmailov et al 2018) exploits the randomness in the optimization algorithms (stochastic gradient descent; SGD). During training, we

often reduce the learning rate after certain iterations, and the model solution does not move much in the loss landscape. SWA with a Gaussian (SWAG; Maddox et al 2019) treats the model samples from the SGD as a Gaussian. Hence, SWAG fits a Gaussian distribution to the local geometry of the posterior:

$$p(\boldsymbol{\theta}|\mathcal{D}) = \mathcal{N}(\boldsymbol{\mu}(\mathcal{D}), \boldsymbol{\Sigma}(\mathcal{D})), \quad (34)$$

where

$$\boldsymbol{\mu}(\mathcal{D}) = \frac{1}{N} \sum_{n=1}^N \boldsymbol{\theta}_n, \quad (35)$$

$$\boldsymbol{\Sigma}(\mathcal{D}) = \frac{1}{N} \sum_{n=1}^N (\boldsymbol{\theta}_n - \boldsymbol{\mu}(\mathcal{D})) (\boldsymbol{\theta}_n - \boldsymbol{\mu}(\mathcal{D}))^T \quad (36)$$

and $\boldsymbol{\theta}_1, \dots, \boldsymbol{\theta}_N$ is the model parameters from the N last iterations. The assumption behind this approach is that the optimizer reaches a reasonably well-established local optimum and only oscillates around it. As a result, the trained parameters $\boldsymbol{\theta}$ represent the targeted relationship equally well.

3.3.4 Applying sampling methods to ECVs

Sampling methods have long been applied to approximate the posterior distributions due to their simplicity of implementation. MCMC and its derivatives such as evolutionary MC (Liang and Wong, 2001) are widely used for marginalizing BDL methods already in earlier epochs. The MCMC algorithms are usually combined with classical MLP models and compared to the deterministic version of the same model. Kingston et al (2005) trained a MCMC MLP to forecast river salinity in the Murray River at Murray Bridge, South Australia. Similarly, Zhang et al (2009) applied MCMC to quantify the uncertainties of steamflow simulations with a specific focus on discussing different treatments of uncertainties, and highlighted the importance of considering variable model architecture and informative prior knowledge for realistic uncertainty quantification. Both of the two mentioned studies reported that the proposed BDL models performed worse than deterministic MLP on the training set but showed superiority in the validation or test set, indicating the difficulty of optimizing a BDL model but also its robustness against overfitting issues. Jana et al (2008) approximated fine-scale soil hydraulic properties in two regional basins based on coarse-scale inputs and also reported better generalizability of MCMC MLP. The uncertainties quantified through MCMC simulations are mostly epistemic, whereas the uncertainties associated with sources other than the model parameters (mostly aleatoric) need to be additionally considered (Humphrey et al, 2016a). Building upon the concept of predictability, Kiani Shahvandi et al (2024c) designed an autoencoder-based architecture and used it alongside Hamiltonian MC (HMC) to prove theoretically and empirically that the uncertainties derived are asymptotically convergent to the aleatoric uncertainties with convergence rate N^{-p} , $\frac{1}{2} < p \leq 1$, where N is the number of MC samples used and p proportional to the difference between two sequential components of the Markov chain.

However, they noted that, in general, the convergence cannot be guaranteed, owing to the potential existence of outliers in the data. In recent years, the rapid growth in hardware capacities has enabled applying MCMC to more complex models such as LSTM for streamflow prediction (Li et al, 2022a), targeting higher spatial resolution of ozone modeling (Sun et al, 2021), or towards a global reconstruction of terrestrial water storage (Rateb et al, 2022). However, the potential for further scaling up the mentioned studies is still limited due to the fact that MCMC increases computational complexity (Sun et al, 2021).

The standing-out disadvantage of MCMC concerning high computational cost has been noted in most of the above-mentioned studies. During the era of large models and big data, MC-Dropout has been increasingly used in practice. Cobb et al (2019) used MC-dropout to quantify the uncertainties associated with their atmospheric retrievals and highlighted the contribution of domain knowledge for achieving realistic uncertainties. Similarly, Tian et al (2022) applied MC-Dropout to quantify the uncertainties associated with their subsurface salinity estimations. However, they emphasized the pitfalls of the assessed uncertainties since the propagation mechanisms remain unclear. MC-Dropout can also be applied to more advanced model architectures without resulting in extremely high computational costs. For example, the coastal ocean time series, including oxygen, nutrients, and temperature, were predicted with satisfactory accuracy with realistic uncertainty information using LSTM by Contractor and Roughan (2021). MC-Dropout is also employed for a more complex model combining convolution and multi-head attention (Gerges et al, 2024) or convolutional autoencoder with skipping connections (Uz et al, 2024) without additional barriers.

3.4 Ensemble approaches

Ensemble approaches are based on a combination of several different models (called ensemble members). Although there are various ways in which models can be defined and combined (Ganaie et al, 2022), three are widely used, namely stacking, bagging, and boosting. In stacking, several models are trained on the same data, and a final model combines the predictions of individual ensemble members. This category can be further separated into two cases, either the model architectures are the same, referring to the well-known deep ensembles (Lakshminarayanan et al, 2017), or combining different model architectures. In bagging, several deterministic models are trained on subsets of the same training dataset, and the final prediction is the average of individual predictions. In boosting, several models are added in a sequential manner, and each ensemble member attempts to correct the predictions of the previous members. In the following, we provide more information on each of these approaches.

3.4.1 Ensemble of different model parameters

Ensemble of different model parameters can be categorized as stacking, where the architectures of the ensemble members are identical. In case a simple averaging based on a prescribed distribution for the input data is used as the final model (being a deep learning model), this type of stacking is referred to as deep ensembles (Lakshminarayanan et al, 2017). A deep ensemble framework involves multiple neural networks

(individual members) sharing the same architecture and optimized using the same strategy. The trainable parameters of each member are initialized stochastically and, therefore, the optimized parameters are different from the rest of the members, forming different basins of attractions, or local optima (Wilson and Izmailov, 2020). The diversity among individual members is enough to quantify the epistemic uncertainties realistically (Fort et al, 2019). The heteroscedastic aleatoric uncertainties can be quantified following Eqs. (18) to (21) for each ensemble member as:

$$\begin{aligned}\mathcal{L}(\boldsymbol{\theta}_i) &= -\log p_{\theta}(\mathbf{Y}|\mathbf{X}, \boldsymbol{\theta}_i) \\ &= \frac{1}{2} \log(\boldsymbol{\sigma}_i^2) + \frac{1}{2} (\mathbf{Y} - \boldsymbol{\mu}_i)^T \text{diag}(\boldsymbol{\sigma}_i^{-2}) (\mathbf{Y} - \boldsymbol{\mu}_i) + \text{constant},\end{aligned}\quad (37)$$

where $\boldsymbol{\mu}_i$ and $\boldsymbol{\sigma}_i^2$ are the mean and variance of the i -th ensemble member. After obtaining M individual models, one can obtain the final prediction and uncertainty as:

$$\boldsymbol{\mu}_* = \frac{1}{M} \sum_{m=1}^M \boldsymbol{\mu}_{\theta_m}, \quad (38)$$

$$\boldsymbol{\sigma}_* = \sqrt{\frac{1}{M} \sum_{m=1}^M (\boldsymbol{\mu}_{\theta_m}^2 + \boldsymbol{\sigma}_{\theta_m}^2) - \boldsymbol{\mu}_*^2}. \quad (39)$$

In practice, it is recommended to train the network to predict the logarithmic variance, $\mathbf{s}_i = \log(\boldsymbol{\sigma}_i^2)$, since this modifies the loss function to:

$$\mathcal{L} = \frac{1}{2} \mathbf{s}_i + \frac{1}{2} \exp(-\mathbf{s}_i) (\mathbf{Y} - \boldsymbol{\mu}_i)^2, \quad (40)$$

which avoids a potential division by zero and is therefore more numerically stable (Kendall and Gal, 2017).

Although deep ensembles have proven as an effective approximation of Bayesian marginalization, they might suffer from the lack of diversity among ensemble members. In this case, repulsive deep ensembles are used (D'Angelo and Fortuin, 2021), in which a 'repulsive' term such as $-|\boldsymbol{\theta}^{(i)} - \boldsymbol{\theta}^{(j)}|$, $j = 1, \dots, T$ is added to Eq. (37), ensuring that $\boldsymbol{\theta}^{(i)}$ and $\boldsymbol{\theta}^{(j)}$ ($i \neq j$) are as different as possible.

3.4.2 Ensemble of different model architectures

The ensemble approach of stacking provides a helpful way of combining the predictions of various models. Since disparate architectures are used in this approach, the algorithm spans the model space to the extent supplied by the practitioner, which might enhance the performance of the deep learning algorithm. The general approach is first to choose the ensemble models and then train them on the same dataset. Finally, the predictions of individual ensemble models are combined to provide the final prediction and its uncertainty, either through a predefined rule (e.g., averaging or maximum voting) or algorithms dedicated to finding the optimal architecture (such as neural

architecture search, Herron et al 2020). Considering M models and denoting them with ϕ_{i,θ_i} , $i = 1, \dots, M$, each with parameters θ_i , and denoting the aforementioned combination and uncertainty computation rule or algorithm as Φ , this ensembling approach can be mathematically represented as:

$$\mu_*, \sigma_* = \Phi(\phi_{1,\theta_1}, \dots, \phi_{M,\theta_m}), \quad (41)$$

Compared to the previously mentioned deep ensembles in Section 3.4.1, an ensemble of different model architectures can explore larger distributions of all possible model parameters and, therefore, may result in better generalizability. However, the risk of mixing the model uncertainties and disparate model capacities exists and potentially results in higher epistemic uncertainties. Moreover, the hyperparameters of individual ensemble members need to be tuned individually, introducing additional workload.

3.4.3 Ensemble of different datasets

Creating ensembles of different datasets is categorized as bagging, although it encompasses boosting as well. This ensemble approach differs from stacking in that it uses the same model for all the ensemble members but trains each identical model on a bootstrapped version of the same dataset. The final prediction and its uncertainty are, respectively, the combination (voting or averaging) of the predictions of individual ensemble members and their spread. The mathematical representation of this ensembling approach is similar to the one presented in Eq. (41), but the model architectures are identical, and the combination rule is simply voting or averaging. Examples of widely used models based on bagging include the so-called Random Forest and Extra Trees. In case ensemble members are added sequentially to correct the predictions of the previous ensemble member, the resulting ensembling approach is termed boosting. In training such models, more attention is paid to the predictions with the largest error to find the required number of ensembles that can predict the training data with arbitrary accuracy.

3.4.4 Applying ensemble approaches to ECVs

Deep ensembles are one of the most widely-used methods for quantifying uncertainties associated with ECVs derived using deep learning algorithms because of their straightforward implementation, superior performance, and even better generalization compared to BNN under domain shift (Izmailov et al, 2021). Using a collection of remote sensing data, Tollenaar et al (2024) used an ensemble of CNN models to detect—with uncertainty—the areas where bare ice is exposed in Antarctica, which provide critical information on the evolution of the ice-sheet. Folino et al (2023) applied deep ensembles to more robustly detect extreme precipitation events, such as those in southern Italy. Similarly, Sha et al (2024) applied deep ensembles for the prediction of severe weather events in the United States. Andersson et al (2021) applied an ensemble of 25 members trained on climate simulations for 6-month-ahead sea ice concentration predictions, outperforming the state-of-the-art dynamical models. The quantified uncertainties are reliable and invaluable for stakeholders to adapt their activities accordingly. The principle of deep ensembles can also be applied to

dynamically average different physical models, which is promising to overcome the deficiencies of individual models (Sengupta et al, 2020). Some studies did not model the aleatoric uncertainties as described in Section 3.4.1, but rather simply retrained the same model multiple times and computed the average for a more robust estimation (López-Puigdollers et al, 2021; Haynes et al, 2024). Moreover, some studies tried to better modeling the aleatoric uncertainties based on input uncertainty information rather than allow the networks to generate by themselves. Gou and Soja (2024) used deep ensembles in the context of data assimilation using deep learning models to enhance the spatial resolution of TWS anomalies derived from GRACE(-FO). This is achieved by incorporating hydrological data through a downscaling approach, resulting in a model that provides accurate and high-resolution TWS anomalies on a global scale. They modified the deep ensemble approach and combined it with MC simulations to account for aleatoric uncertainties caused by input data uncertainties, also during inference. However, they noted that not all the relevant input uncertainties might be captured and, therefore, the estimated uncertainties might be overly optimistic. This approach is further discussed in Section 3.5. Furthermore, some studies attempted to benefit from multiple ensembling principles. Liu et al (2023) trained multiple spatiotemporal models for wind speed forecasting and also trained based on different training datasets. They also let the model directly output associated uncertainties. Therefore, their approach is a combination of all the three types of ensembles mentioned in this section and achieves high-precision point prediction with reliable probabilistic information.

Ensemble of different model structures also shows benefits in various fields in geosciences (Natras et al, 2022), including in ECV studies. For instance, Jose et al (2022) used an ensemble of six different machine learning models to provide accurate daily forecasts of precipitation and temperature over the Western Ghats region in India. They demonstrated significant improvement compared to the forecasts based on traditional general circulation models. Du et al (2023) applied five different ensemble models to map the land cover in the Xinjiang region in northwest China. They showed a better performance of their ensemble algorithm compared to that of the individual models, thereby providing incentive for the utilization of ensemble learning for land cover mapping in arid areas that are subject to increased attention under the ongoing climate change. Although the stacking approach has gained increasing attention, it might suffer from the same ailments as deep ensembles (i.e., lack of diversity among ensemble models), as well as being computationally expensive to implement. Moreover, the discrepancies among different ensemble members can be relatively large since the individual model architecture may have different capacities.

Bagging has also been applied to ECV studies but more often combined with machine learning models, such as tree-based models, rather than deep neural networks. Heydari et al (2024) analyzed the performance of several boosting models (including XGBoost and Gradient Boosting Machine) for water quality forecasts in Prespa Lake in Greece. They demonstrated the effectiveness of boosting in their study, which is in agreement with the general usefulness of boosting in hydrological problems (see e.g., Zounemat-Kermani et al, 2021). Malakouti (2023) applied several bagging and boosting models for the prediction of global temperature change and showed that in this

problem, Extra Trees (a bagging model) presented the best prediction performance. Hence, ensembling based on bagging or boosting is advantageous in ECV problems. Also, combinations of these approaches with stacking yield promising results. For example, [Zaier et al \(2010\)](#) combined boosting and stacking based on multiple MLP models for more accurate lake ice thickness estimations.

3.5 Explicitly considering data uncertainty in a deep learning model

As described above and already mentioned in Section 1, the majority of investigations about uncertainty quantification in deep learning models focus on epistemic parts but do not pay the same amount of attention to data quality ([Gruber et al, 2023](#)). More specifically, the uncertainties caused by input data, especially during inference, are largely ignored. It is possible to dynamically weigh the loss values of individual samples or batches based on the available label uncertainty information ([Kiani Shahvandi and Soja, 2022](#)) or based on certain criteria ([Gou et al, 2024](#)) for a more robust estimation, sharing the similar strategy as Eq. 8 in the conventional statistical model. However, the predictive uncertainties caused by the input features are still missing. One of the reasons may be the fact that typical datasets for vision and language modeling tasks, which inspired the majority of deep learning developments, are not associated with uncertainty information (see, e.g., [Deng et al, 2009](#)). On the contrary, the classical statistical approaches (Section 2.3.1) commonly used by geoscience and climate scientists emphasize uncertainty propagation, namely the consequence of input uncertainties on the estimations based on a given model. As a result, applying mature and established uncertainty quantification approaches developed based on classical deep learning tasks, such as vision and language processing, to ECV studies may result in the loss of crucial information, especially considering the varying real-world situations and the inherent measurement noises of satellite systems ([Gawlikowski et al, 2023](#)). It is relevant to explicitly consider the data uncertainty, whenever they are available, in a deep learning model for reaching realistic uncertainty information.

[Jungmann et al \(2024\)](#) proposed an analytical solution to propagate aleatoric uncertainties caused by the inherent input uncertainties through a neural network by utilizing the law of uncertainty propagation and provided rigorous theoretical results. In theory, this method is computationally efficient since it only needs the parameters of the network, with the only prerequisite that the neural networks should be continuously differentiable. The non-fully-connected layers, such as convolution and pooling layers, need to be expressed as vector-matrix multiplication to ensure mathematical rigor. In practice, the differentials can be obtained by using automatic differentiation engines ([Abadi et al, 2015](#); [Paszke et al, 2019](#)). As an alternative, we can benefit from sampling methods. Test-time augmentation ([Ayhan and Berens, 2018](#)) is a useful tool for quantifying the aleatoric uncertainties by applying augmentation principles to generate test samples. To this end, augmentation techniques are used to mimic the distribution of the test set so that the impacts of input uncertainties can be estimated. The motivation for this approach is that images are normally not associated with quantified uncertainties. Therefore, augmentation techniques are used to mimic the possible errors of the input images so that the output uncertainties can be quantified

(Wang et al, 2019). Loquercio et al (2020) proposed a framework to explicitly consider the data uncertainties by propagating them using assumed density filtering (Boyen and Koller, 2013). Then, the data uncertainties are combined with model uncertainties quantified using MC-Dropout to quantify the total uncertainty. The proposed method is not dependent on the network architecture and task, does not change the optimizing process, and can be applied to an already trained model.

Similar sampling strategies can be applied to overcome the limitation of the classical deep ensembles approach: the aleatoric uncertainties are directly generated by the networks without sensing the real uncertainty information of the input data \mathbf{X} . Therefore, the heteroscedastic uncertainty may differ from the real ones caused by the input errors. The limitation can be circumvented by combining deep ensemble and Monte Carlo sampling approach to better utilize the uncertainty information of inputs during inference (Gou and Soja, 2024). The basic procedure remains the same as for classical deep ensembles (Section 3.4.1), but now the model gives one output, namely the predicted mean ($\boldsymbol{\mu}$). The individual ensemble members can be optimized based on the classical loss functions, which can simplify the loss landscape and may stabilize the optimization process. Once all the individual members are trained, Monte-Carlo simulations are performed during inference based on each of them. The first step is to sample from the distribution of the inputs based on their uncertainty information:

$$\mathbf{x}_i^* \sim \mathcal{N}(\mathbf{x}^*, \boldsymbol{\sigma}_{\mathbf{x}^*}^2). \quad (42)$$

Then, the Monte Carlo simulations are run I times and quantify the aleatoric uncertainties as follows:

$$\boldsymbol{\mu}_{\theta_m}^* = \frac{1}{I} \sum_{i=1}^I \boldsymbol{\mu}_{\theta_m, i}^* = \frac{1}{I} \sum_{i=1}^I f(\mathbf{x}_i^* | \theta_m), \quad (43)$$

$$\boldsymbol{\sigma}_{\theta_m}^* = \sqrt{\frac{1}{I} \sum_{i=1}^I (\boldsymbol{\mu}_{\theta_m, i}^* - \boldsymbol{\mu}_{\theta_m}^*)^2}, \quad (44)$$

and obtain the final predictions and uncertainties by putting Eqs. (43) and (44) into Eqs. (38) and (39). Quantifying the heteroscedastic uncertainties using MC simulations has a similar philosophy as a sensitivity analysis (see, e.g., Hofer, 1999; Cacuci and Ionescu-Bujor, 2004; Gou et al, 2023) that are used in quantifying uncertainties of complex systems (Appendix B). To this end, the epistemic uncertainty is quantified in the same way as with classical deep ensembles, namely exploring the different modes in the function space. However, the aleatoric uncertainty is now explicitly dependent on the input uncertainties, which are supposed to provide more realistic uncertainty information and better address the needs of handling sEO data.

3.6 Other advancements in the era of large models

In previous sections, we described multiple widely used uncertainty quantification approaches. These approaches can be categorized into three classes, with the caveat

that these are not necessarily the only methods available but are specifically highlighted due to the nature and purpose of the present survey. For a more comprehensive review of existing deep learning techniques for uncertainty quantification, we refer to topical survey papers, such as the ones by [Abdar et al \(2021\)](#) or [Gawlikowski et al \(2023\)](#). In this section, we include some recent developments specifically designed for the era of large models with big data. They are becoming increasingly critical in the context of applying deep learning models to quantifying ECVs on a global scale and considering complex climate systems ([Schneider et al, 2023](#); [Bi et al, 2023](#); [Zhang et al, 2023](#); [Lam et al, 2023](#)). The recent efforts towards establishing Earth and climate foundation models also highly desire the realistic approaches for quantifying uncertainties ([Zhu et al, 2024](#); [Tuia et al, 2024](#); [Bodnar et al, 2024](#)). The potential for overcoming the difficulty of applying methods like MCMC to a larger scale due to future boost of computational resources has been expected in previous studies ([Kingston et al, 2005](#)) but has not come true since the modern developments are towards significantly larger models. The complexity of the model architectures and the data volume have been increasing dramatically, along with the evolution of computational resources. Therefore, approximating the full distributions of all trainable parameters (Section 3.2) or sampling the posterior distributions based on Markov Chain (Section 3.3) are not affordable. Even training complete models several times to formulate deep ensembles becomes costly. With this background, multiple studies investigated the proxies of ensembles by only stochastically varying parts of the deep learning model to quantify epistemic uncertainties. To this end, de-correlated predictors that can sample the weight distributions may be obtained without training and storing copies of the complete networks and large training datasets in memory. [Turkoglu et al \(2022\)](#) introduced FiLM-Ensemble, which is based on the concept of feature-wise linear modulation to generate an ensemble to provide well-calibrated epistemic uncertainties implicitly. [Halbheer et al \(2024\)](#) proposed low-rank adaptations (LoRA) to replace the respective linear layers with custom LoRA modules and generate varying predictions. Both studies can be understood as an implicit ensemble, which can provide realistic epistemic uncertainties without the need to repeat training the whole model. Both studies have not been applied to ECV studies but have already been comprehensively examined on classical computer vision datasets, where they have shown potential for application to ECV-related studies. The diffusion probabilistic models ([Ho et al, 2020](#)) have recently gained numerous successes, and their probabilistic nature is beneficial for quantifying uncertainties in weather forecasting model ([Price et al, 2023](#)) or land surface model ([Lu et al, 2024](#)).

4 Applications

In this section, we apply selected BDL approaches to two real-world ECV estimation use cases to discuss the resulting uncertainties. Since the previous survey on existing studies in Section 3 involves various ECV parameters and spreads across a wide range of the Earth system, quantitative discussion about different uncertainty quantification approaches is difficult. The two application cases in this section intend to provide straightforward feelings on the characteristics of the aforementioned methods. Section 4.1 discusses the results for SCF estimations based on deep ensembles and focuses on the fidelity of the estimated uncertainties compared to actual errors. Section 4.2 discusses the results for TWS change estimations based on four selected deep learning approaches introduced in Section 3 and focuses on the differences and similarities of resulting uncertainties. In addition, the uncertainties derived from least-squares estimation are also included for comparison.

4.1 Snow cover

Snow cover is recognized as an ECV due to its significant impact on the Earth's climate system and hydrological cycles. It affects the albedo, or reflectivity, of the Earth's surface, which in turn influences global and regional temperatures by reflecting or absorbing sunlight. Snow acts as a natural insulator and water reservoir, releasing freshwater during warmer months, crucial for drinking water, agriculture, and hydroelectric power. Changes in snow cover also affect weather patterns, ecosystem dynamics, and climate feedback mechanisms, making it integral to climate modeling and predictions. Information about the snow cover is important for several applications, including climate change (Brown and Robinson, 2011) and environmental monitoring (Sturm et al, 2001), water resource management (Sturm et al, 2017), and forecasting hazards such as avalanches (Eckert et al, 2024) and floods (Yan et al, 2023). Various techniques for surveying the snow coverage on regional and global scales exist. Meteorological observations and regular manual surveys of snow depth and snow density are traditional methods to estimate the snow water equivalent and to track the evolution of the snow cover. Contrary to the meteorological observations, satellite images provide continuous spatial measurements, acquired globally at regular intervals. During the last decades a number of methods for snow-cover mapping have been developed for optical as well as for active and passive microwave sensors (Hall et al, 2002; Tsai et al, 2019; Pulliainen et al, 2020). Because the spatial resolution of the satellite images from today's passive microwave sensors is coarse (5–25 km), and the active microwave sensors may struggle to provide reliable information about the snow (Tsai et al, 2019), optical images from sensors like MODIS, AVHRR and Sentinel-3 SLSTR are often applied in both regional and global snow monitoring (Hall et al, 2002; Hüsler et al, 2014; Solberg et al, 2021).

The [ESA Snow_cci project](#) aims to contribute to the understanding of snow in the climate system by generating consistent, high quality, long-term datasets that meet the requirements of the GCOS. The objective of Snow_cci is to generate homogenized long-time series of daily global snow extent maps from optical satellite data and daily global snow water equivalent products from passive microwave satellite data. In addition, the

project aims to generate corresponding, pixel-wise uncertainty products. To describe the snow extent, Snow_cci uses the SCF variable. The methodology for estimating SCF is based on the SCAMod algorithm (Metsämäki et al, 2012), which is based on a forward semi-empirical model where the at-satellite observed reflectance is expressed as a function of the fractional snow cover. For estimating the uncertainty, an error propagation approach has been applied for MODIS and SLSTR sensors (Salminen et al, 2018).

4.1.1 Overview of data and models

In the following, we present an application similar to the ESA Snow_cci SCF estimation, but using a deep learning-based method to estimate SCF and the corresponding aleatoric, epistemic, and total predictive uncertainties. Our study area includes the Scandinavian Peninsula, where we define the area of interest to encompass Norway and Sweden, and the European Alps region. The data source for product generation is the Sentinel-3 Sea Land Surface Temperature Radiometer (SLSTR), which is based on the heritage of Envisat’s Advanced Along Track Scanning Radiometer. SLSTR observes in two directions and has a swath width of 1675 km (nadir) and 750 km (backward). The sensor provides observations over Scandinavia at least once a day. The instrument has nine bands in the spectral range 0.55 to 12 μm , but we consider only the bands S1 (554.27 nm), S2 (659.47 nm), S3 (868.00 nm), S5 (1613.40 nm) and S6 (2255.70 nm). We are not using bands S4 (1374.80 nm) and S7 (3742.00 nm) since we experienced, at several occasions, data of lower quality in these bands.

The Sentinel-2 Multi Spectral Instrument (MSI) is the main source of reference data as it is expected to be closest to ground truth due to its high-resolution data. Physics-based algorithms are used for retrieval, and the high resolution provides the ability to visually evaluate the results, including snow cover, by an experienced operator. The Sentinel-2 and Sentinel-3 images that were selected for training data generation were subject to automatic cloud detection and subsequent manual inspection to mark areas with erroneous cloud detection. We have chosen an accurate binary snow-cover algorithm (Klein et al, 1998) to generate reference SCF maps from Sentinel-2 MSI. The binary result was checked against a pseudo-color image based on a combination of MSI bands making maximum contrast between snow-covered and snow-free areas by an image interpretation expert. The high-resolution image was then down-sampled by averaging to Sentinel-3 SLSTR resolution in order to be applied to train the U-Net for pixel-wise mapping of SCF from Sentinel-3 SLSTR data.

The data set was divided into training and test sets: The years 2016 and 2017 are used for training the deep learning model and the year 2018 is used for testing. To create the input-label pairs, the reference snow products were paired with Sentinel-3 images as follows:

- Find SLSTR images that were recorded ± 24 hours compared to the Sentinel-2 reference image used to create the reference product,
- Remove pairs where the SLSTR image has an overlap of less than 40% of the reference product,

- Re-project the reference product onto the same grid as the SLSTR image using nearest neighbor interpolation and crop the SLSTR product to the rectangle enclosing the reference product with a 128 pixels margin,
- Apply automatic cloud detection to the SLSTR data (Metsämäki et al, 2015) and mask out cloud pixels in the reference product by inserting a value representing "unknown",
- Remove any resulting pairs with less than 20 pixels not labeled as "unknown".

The model architecture used for single task problems is a slightly altered version of the U-Net proposed by Ronneberger et al (2015). The network consists of an encoder and a decoder, each of which consisting of a basic building block of three convolutional layers, with subsequent batch normalization and a ReLU-activation function. The convolutions are implemented with the padding-scheme proposed by Liu et al (2018), called partial convolutions, to reduce edge effects. In the encoder part, the images go through four such blocks with down-sampling by a factor of two after each block. In the decoder part, the resulting feature maps are subject to four such blocks with a bi-linear up-sampling operation after each, also with a factor of two. The feature maps go through one more block with convolutions before the final two separate convolution layers that map to the desired snow cover fraction and aleatoric uncertainty (see Section 3.4.1), respectively. Between the encoder and decoder, high-resolution feature maps are bypassed to let the network also make use of local high-resolution information. The training was conducted using 80,000 iterations with a batch size of 32 samples. The batches were created by drawing random 128×128 sub-crops from the training set. We used the Adam optimizer (Kingma and Ba, 2014) with a learning rate of 0.0001.

4.1.2 Deep ensemble results

A ten-member ensemble was created by training ten individual U-Net models to estimate the SCF values, together with the aleatoric and epistemic uncertainties as outlined in Section 3.4.1. The fidelity of these uncertainties was evaluated by categorizing the estimated SCF into 10 bins, calculating the average estimated SCF, and comparing it with the average target (ground truth) SCF for each bin using the test samples. The results indicate a strong correlation between the average estimated and target SCF values (Fig. 3a). Similar calculations applied to the uncertainty measurements reveal a close alignment between the total uncertainty (Eq. (39)) and the unbiased root mean squared error (RMSE) with respect to ground truth, albeit with a slight deviation in the unbiased RMSE compared to the total uncertainty (Fig. 3b). Further analysis shows that uncertainties are lowest at high and low SCF values, with aleatoric uncertainty consistently higher than the epistemic uncertainty. Distribution comparisons between the total uncertainty and the unbiased RMSE demonstrate that the former exhibited a heavier right tail, suggesting potential spikes in estimated uncertainties (Fig. 3c). To assess the performance further, we divide the estimated total uncertainty into 10 bins and compute the average aleatoric and epistemic uncertainties, and the average unbiased RMSE for each bin. The results indicate a very good correspondence between the average total uncertainty and the average unbiased

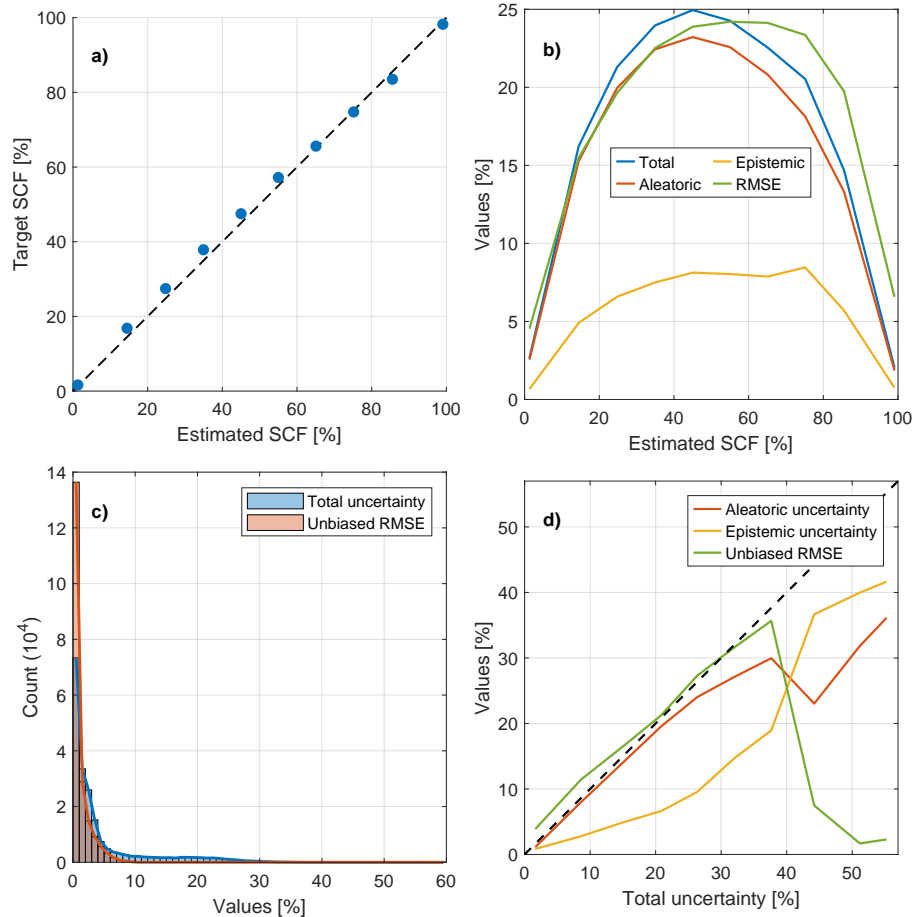


Fig. 3: SCF estimations and their uncertainties. (a) Estimated SCF compared with ground truth. (b) Estimated SCF compared with epistemic, aleatoric and total uncertainty estimates and the unbiased RMSE. (c) Distribution of total uncertainty and unbiased RMSE. (d) Total uncertainty compared with aleatoric and epistemic uncertainties and unbiased RMSE.

RMSE for total uncertainty values less than 38 % (Fig. 3d). However, for total uncertainty values exceeding 38, the unbiased RMSE decreases, with epistemic uncertainty becoming predominant at higher total uncertainty levels.

An example from April 12, 2018, a cloud-free day across much of the study area, reveals low aleatoric and epistemic uncertainties in regions with high estimated SCF, including forested areas (Fig. 4). The highest uncertainties are noted near the snow line, such as in southern Sweden. Across the study area, the aleatoric uncertainties are in general higher than the epistemic ones. Examination of the uncertainty maps in Fig. 4 indicates similar spatial patterns in both types of uncertainty in the sense that the aleatoric uncertainty has high values at the same locations as the epistemic

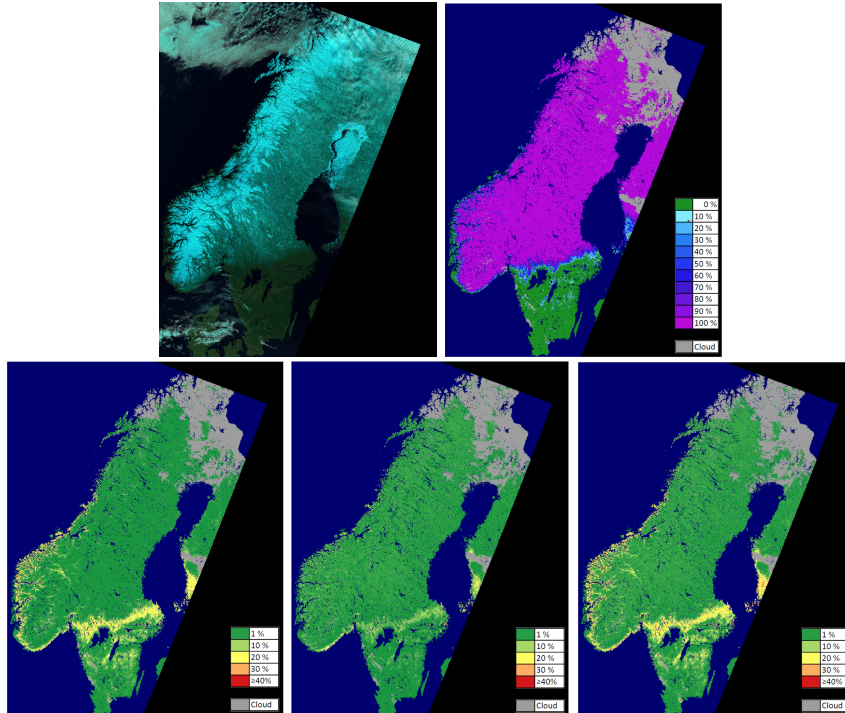


Fig. 4: SCF estimation results and associated uncertainties obtained from deep ensemble for April 12, 2018. Upper-left: Sentinel-3 SLSTR data. Upper-right: Estimated SCF values. Lower-left: Aleatoric uncertainties. Lower-center: Epistemic uncertainties. Lower-right: Total uncertainties.

uncertainty has high values. This aligns with the findings in [Kahl et al \(2024\)](#), which demonstrated that, while separation of aleatoric and epistemic uncertainties is effective with simulated data, it may not directly translate to real-world scenarios.

To further demonstrate uncertainty estimation using deep ensembles, we applied the deep learning model trained exclusively on Scandinavian data, to estimate SCF and corresponding uncertainties in the European Alps (Fig. 5). Despite the lack of reference data for quality assessment and the absence of water and cloud masks, visual inspection suggests that the model accurately maps snow coverage in the Alps. However, it incorrectly predicts snow north of the Alps and misclassified clouds as snow (Fig. 5, upper-right), likely due to the lack of cloud data in the training dataset and a domain shift in land cover and terrain between Scandinavia and the Alps. Yet, when inspecting the corresponding uncertainty maps, we observe that most of these erroneous classifications have high uncertainties. Similar to the Scandinavian test case, we observe that for lower SCF estimates, the aleatoric uncertainties are typically higher than the epistemic ones. However, for cloud objects we often observe higher epistemic uncertainties (Fig. 5) with different patterns than the aleatoric uncertainties, contrary to the Scandinavian case. This phenomenon demonstrates that the main reason for

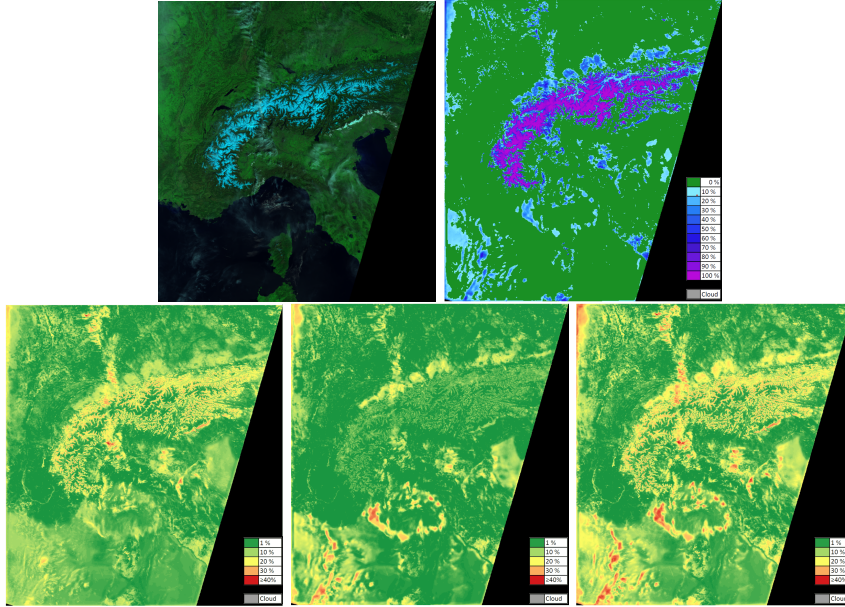


Fig. 5: Results of deep ensemble uncertainties for the European Alps on April 6, 2024. Upper, left: Sentinel-3 SLSTR. Upper, right: Estimated snow cover fraction. Lower, left: Aleatoric uncertainty. lower, center: Epistemic uncertainty. Lower, right: Total uncertainty of SCF estimates.

epistemic uncertainties in a deep learning model is an incomplete coverage of the training data distribution. Tests on images with higher cloud coverage often result in thick cloud interiors being mistakenly estimated as 100 % SCF, with near-zero corresponding uncertainties. Such scenarios have huge dataset shifts compared to the training data, and the findings support the conclusions of [Ovadia et al \(2019\)](#) that the quality of the uncertainty products degrades with increasing dataset shift, despite the relative robustness of deep ensembles to such shifts.

4.2 Terrestrial water storage changes

4.2.1 Overview of data and models

In the second application case, we designed an experiment to predict the terrestrial water storage changes based on hydrological variables and focus on discussing the uncertainties quantified from different deep learning models. The problem setting is motivated by the water balance equation, which describes the relationship between the changes of TWS (TWSC) and precipitation (P), evapotranspiration (ET) and runoff (R):

$$\text{TWSC} = P - ET - R, \quad (45)$$

where TWSC can be obtained from GRACE-measured TWS anomaly (TWSA) by computing centered finite differences:

$$\text{TWSC}_t = \frac{\text{TWSA}_{t+1} - \text{TWSA}_{t-1}}{2\Delta t}, \quad (46)$$

with t_1 , t , $t + 1$ denoting three consecutive months, and Δt denoting one month. The missing months within the study period were filled using cubic interpolation. The data were collected by [Lehmann et al \(2022\)](#), including 11 sets of precipitation and runoff data and 14 sets of evapotranspiration data with different temporal coverage. Based on the temporal intersection of these datasets and the GRACE satellite mission, we selected data from January 2003 to December 2014. To reconcile the different spatial resolutions of the used datasets and suppress included outliers, basin-wise average time series in 189 river basins defined by the Global Runoff Data Center ([GRDC, 2020](#)) were generated. We used the ensemble average of all the mentioned datasets as the input and their standard deviations as associated uncertainty information for our deep learning approach. The standard deviations of individual products can usually result in relatively realistic uncertainty estimates but may also overestimate them due to the presence of outliers ([Tarek et al, 2021](#); [Goswami et al, 2024](#)). The average uncertainties of the three hydrological parameters of the 189 basins, both absolute and relative compared to the average signal levels in terms of standard deviations, are shown in [Fig. 6](#).

Considering the high-frequency artifacts that may be introduced by simple forward or backward differences ([Landerer et al, 2010](#)) and different decaying of the daily fluxes in the storage ([Humphrey et al, 2016b](#)), we selected an input sequence of 11 months ($t - 5, \dots, t, \dots, t + 5$) to model the TWSC at the central month (epoch t) as the target. This problem setting allows the models to overcome the high-frequency artifacts based on optimization while considering the intra-annual signals, which should cover the varying water storage memories in most basins. To this end, we obtained 24'948 samples from January 2003 to December 2013 (132 months) and further split them into training set from January 2003 to December 2010 (96 months, 18'144 samples) and test set from January 2011 to December 2013 (36 months, 6'804 samples).

We selected four deep learning models, including MC-Dropout ([Sec. 3.3.2](#)), BNN ([Sec. 3.2.1](#)), deep ensemble (DE; [Sec 3.4.1](#)) and combining deep ensemble and Monte Carlo simulations (DEMC; [Sec. 3.5](#)). We further applied the least-square adjustment to estimate the linear relationship between the 33 input features and the one target to

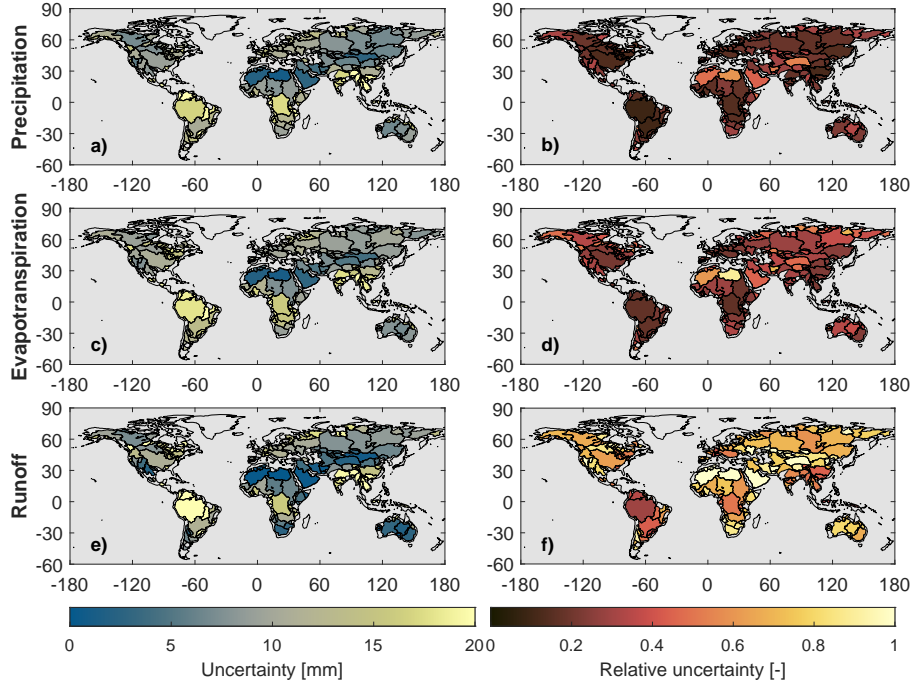


Fig. 6: The uncertainties (left) and the ratio of uncertainties w.r.t. signal levels (right) of the three hydrological variables across multiple products.

show the quantified uncertainties in a conventional statistical model. The comparison focuses on the characteristics of obtained uncertainties using different techniques but refrain from evaluating the performance in terms of accuracy. The model architectures of different models and the optimizing strategies stay the same to ensure a relatively fair comparison among the different candidates. We designed an MLP model with five layers. The first layer (input layer) projects 33 features into a 256-dimensional hidden state and feeds to three hidden layers with 256 neurons. The last layer (output layer) projects the final hidden state into two outputs, representing the targeted TWSC at epoch t and its associated aleatoric uncertainty. The final layer of the DEMC model is slightly different since it only provides one output representing the targeted TWSC at epoch t (Sec. 3.5). All the layers except for the output layer are followed by a $\text{ReLU}(x) = \max(x, 0)$ activation function. All the models were implemented in PyTorch V2.1.0 (Paszke et al, 2019) and optimized using Adam (Kingma and Ba, 2014). Specifically, the BNN model has been realized using a publicly available implementation by Lee et al (2022).

4.2.2 Comparing the quantified uncertainties using different methods

Fig. 7 shows the average total predictive uncertainties and prediction errors in terms of RMSE over the three-year test interval. All the deep learning methods provide plausible uncertainties with BNN and MC-Dropout tending to provide relatively higher uncertainty estimates than DE and DEMC. The uncertainties estimated by the least-square model are slightly lower than others and tend to be over-optimistic (Fig. 7i and j). The unconsidered epistemic uncertainties likely cause this underestimation, as discussed in Section 2.3.1.

We further analyze the relationship between prediction errors and the predictive uncertainties of individual samples, namely individual months in all 189 basins. Table 2 shows the percentage of prediction errors lying within the corresponding confidence interval. All the deep learning methods have similar confidence intervals, with MC-Dropout tending to overshoot the prediction errors, whereas the least-square model clearly underestimates the total uncertainties. The deep learning methods typically have a wider $1\text{-}\sigma$ confidence interval but a narrower $3\text{-}\sigma$ interval compared to a Gaussian distribution, indicating that the distribution of errors is not fully Gaussian but with long-tail outliers, which cannot be avoided in real-world applications.

Table 2: The percentages of prediction errors that lie in the confidence intervals for the five models considering their quantified uncertainties. The reference confidence intervals by assuming a Gaussian distribution are 68 %, 95 %, and 99.7 %, for one, two, and three standard deviations, respectively.

	Training set			Test set		
	$1\text{-}\sigma$	$2\text{-}\sigma$	$3\text{-}\sigma$	$1\text{-}\sigma$	$2\text{-}\sigma$	$3\text{-}\sigma$
BNN	76.1 %	96.8 %	99.5 %	67.7 %	93.1 %	98.8 %
MC-Dropout	79.6 %	97.4 %	99.6 %	72.1 %	95.1 %	99.2 %
DE	75.3 %	96.2 %	99.3 %	67.3 %	93.0 %	98.6 %
DEMC	75.8 %	94.7 %	98.5 %	66.7 %	91.2 %	97.6 %
LSQ	66.4 %	89.7 %	96.3 %	61.7 %	88.1 %	95.9 %

Fig. 8 further extends the analysis by showing the aleatoric and epistemic uncertainties separately. It is worth noting that the aleatoric uncertainties provided by BNN, MC-Dropout, and DE models are directly generated by the network based on Eqs. (18) to (21), while the ones from DEMC were generated based on sampling considering the input uncertainties, see Eqs. (43) and (44). Aleatoric uncertainties with marginal contributions from the epistemic uncertainties dominate the total predictive uncertainties of all four tested deep learning models. The results prove the efficiency of the tested non-BNN proxies since they provide epistemic uncertainties that are close to those of the BNN ones. Moreover, the low epistemic uncertainties suggest that the training set has relatively good coverage of the whole data distribution and, therefore, the model has good generalizability. Only MC-Dropout provides slightly higher epistemic uncertainties, which are due to the varying model architecture as described in

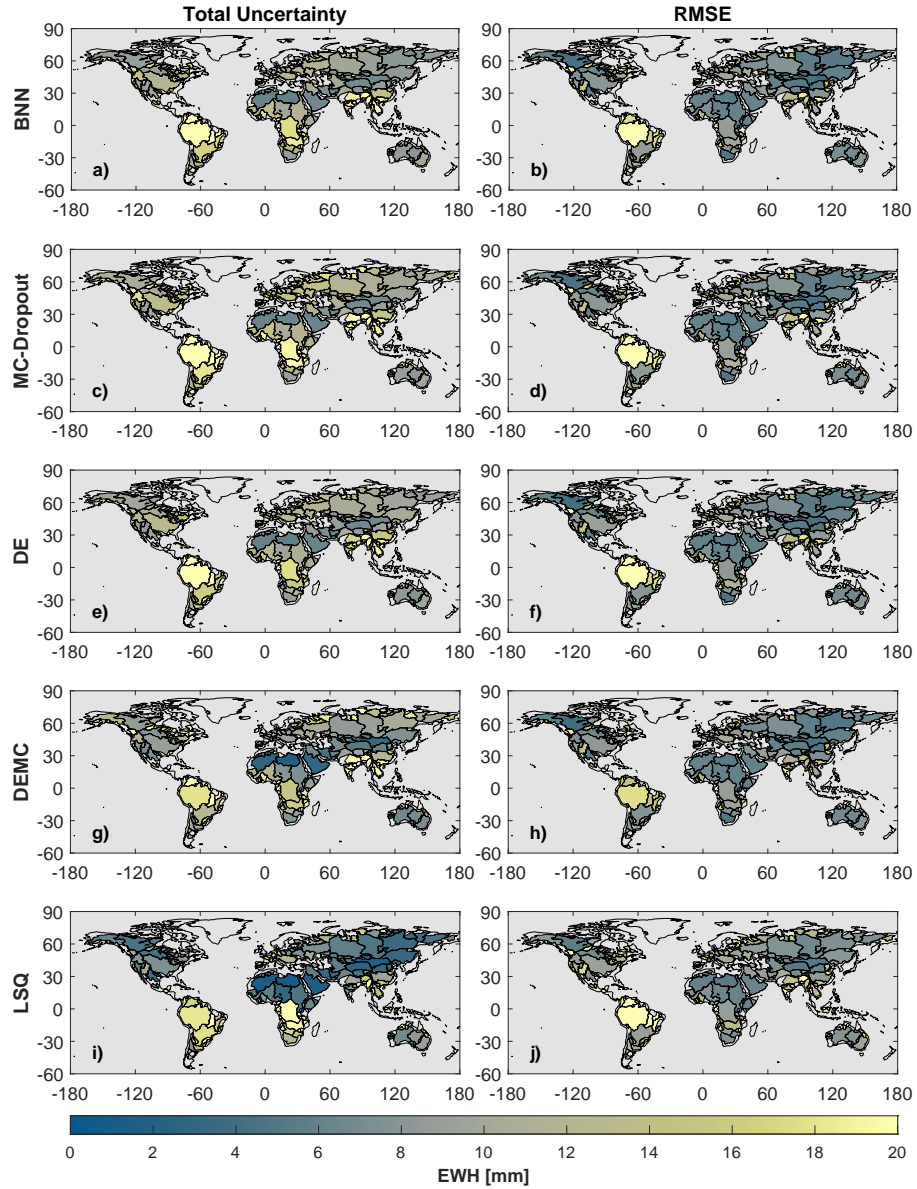


Fig. 7: Comparison of the total predictive uncertainties (left) and errors of the predictions (right) in the 189 basins. The five rows show the results using four deep learning models and least-square estimation (LSQ). All the values are in the format of equivalent water height (EWH) with millimeters as units.

Section 3.3.2. The dominating role of aleatoric uncertainties in this application case is similar to the previous snow example in the Scandinavian Peninsula and opposite to the European Alps case. This application case indicates the potential risk of

heavily underestimating the quantified total predictive uncertainties if the aleatoric uncertainties are not rigorously considered.

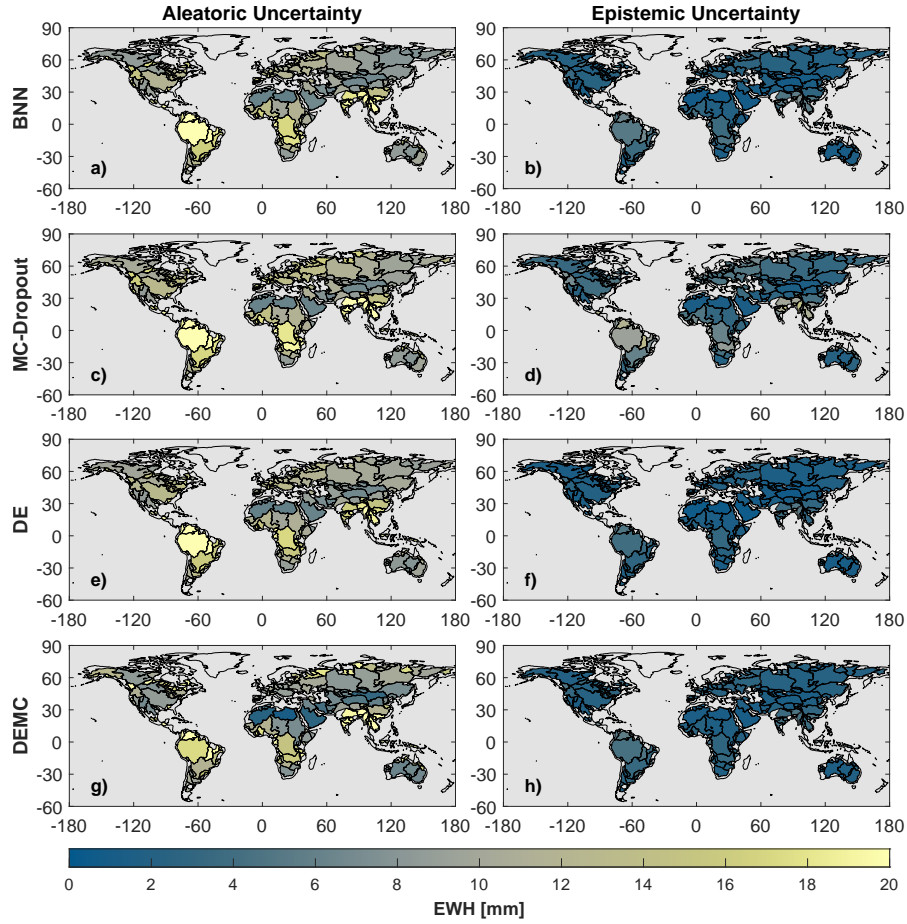


Fig. 8: Comparison of the aleatoric uncertainties (left) and epistemic uncertainties (right) in the 189 basins. The four rows show the results using four different deep learning models. All the values are in the format of equivalent water height (EWH) with millimeters as units.

Also noteworthy are the different patterns of aleatoric uncertainties. Aleatoric uncertainties estimated by the DEMC model show slightly different patterns than the other three models. Higher aleatoric uncertainties are reported by DEMC for the basins in North America, including the Fraser Basin, Churchill Basin, and other small basins surrounding Hudson Bay, as well as for the basins in Northern Siberia. This effect results from higher runoff uncertainties in those basins (Fig. 6e). The results demonstrate the ability of DEMC to provide realistic uncertainty information by explicitly

considering input uncertainties, whereas the other methods tend to underestimate the total uncertainties in these regions (Fig. 7). Therefore, DEMC can alert potential inferior estimations when the inputs are associated with high uncertainties, which is valuable for satellite-based variable parameter estimations, as long as we have access to input uncertainties.

5 Conclusions and Future Perspectives

5.1 Conclusions

Reliable uncertainty information is critical for decision-making, adding value to results and making them trustworthy. This survey starts with the theoretical foundations of uncertainties to discuss the similarities and differences between conventional statistical and deep learning perspectives on problem setting and uncertainty quantification. The main takeaway is that the conventional statistical view assumes that the predefined relationship based on domain knowledge is correct, so all the uncertainty should stem from input data randomness. Although the deep learning perspective also presumes the existence of a relationship between inputs and targets, the functional expression of such a relationship is considered unknown and empirically estimated from large training datasets using a model with sufficient capacity. Deep learning users aim to understand the deficiency of the models (epistemic uncertainties) and allow the model to quantify the data uncertainties (aleatoric uncertainties) based on the overall data distribution, while typically ignoring the quality of individual samples. Both perspectives are based on the different nature of the respective problem settings. Applying deep learning algorithms to sEO data for ECV estimation is an interdisciplinary problem intersecting classical Earth science and advanced data-driven methods. Hence, we need to bridge the different perspectives and combine them to consider their individual strengths and limitations so that we can fulfill the requirements from both sides. The geoscience and climate scientists can benefit from the matured uncertainty quantification approaches developed for typical deep learning tasks such as vision and language modeling (Abdar et al, 2021; Gawlikowski et al, 2023), with some specific modifications aimed at solving specific ECV-related problems.

In Section 3, we provide a thorough discussion on the different properties of various deep learning methods with examples from previous ECV studies. This discussion provides a basis for selecting suitable deep learning methods for the specific requirements of a certain task. Furthermore, this study applied selected BDL techniques to two real-world cases of ECV retrieval to provide quantitative assessments of uncertainties obtained from different approaches and demonstrates that the different BDL methods work equally well with marginal differences among them. However, this may be a partial conclusion since we only tested two cases, which do not represent the entire Earth system. An important conclusion is that we cannot neglect either aleatoric or epistemic uncertainties since the dominating role varies across different applications, and even specific cases. It is highly recommended that both types of uncertainties be rigorously quantified to provide realistic total uncertainties unless there is strong evidence that one of them is negligible. Explicitly considering the input feature uncertainties when quantifying the predictive uncertainties has proven beneficial for ECV applications. Whenever such information is available, it should thus be considered. On the other side, the conventional least-square adjustment based on predefined functional relationships clearly underestimates the predictive uncertainties in our application case, highlighting the impact of ignoring epistemic uncertainties.

5.2 Future perspectives

One of the major concerns about using sEO products derived from deep learning techniques is the "black-box" nature of deep learning algorithms. These characteristics impede users from understanding the model, which can lead to doubts about the results, especially when making sensitive decisions. Realistic uncertainty quantification enhances trust in the results and, furthermore, can be seen as a contribution to explainable AI (Roscher et al, 2020; Samek et al, 2021). Interpretable machine learning has been gaining increasing attention in the field of geoscience to avoid potential risks caused by superficial applications and better utilize the potential of machine learning (Jiang et al, 2024a; Kiani Shahvandi et al, 2024b).

Another concern that needs to be addressed is the appropriate consideration of input data uncertainties. It is overly optimistic to expect a world where all sources of uncertainty are known. However, uncertainty information is more likely to be available for sEO datasets than for data types typically used in deep learning tasks, such as texts and photos. Therefore, explicitly considering the input uncertainties for both ECV retrieval and associated uncertainty quantification should be promoted. Geoscientists and climate scientists may take the responsibility to develop suitable tools for this purpose since this direction may not fully align with the priorities for vision and language modeling applications, in which the data uncertainties are typically inaccessible.

Another important development is to combine physical information and data-driven approaches, for example, in the form of physics-informed neural networks (PINNs; Raissi et al 2019) or physics-constraint neural networks. When we have strong confidence in physics-based relationships and believe they are suitable for the specific application, we can impose this prior knowledge to enhance the performance of models (e.g., Kiani Shahvandi et al, 2024a). We can either apply the constraints to the model parameters (the principle of PINNs) or the model predictions—the latter shares similar logic with the condition matrix \mathbf{B} in a least-square adjustment. Alternatively, we can formulate the loss function based on such a relationship and convert a regression problem into a parameter estimation problem (Kutz, 2023). To this end, we constrain the model parameters so that they are not entirely free to take arbitrary values from the parameter space but are forced to converge to the solutions fulfilling the physical relationships. With these developments, we may reduce the uncertainty by benefiting from the well-established relationship and also possibly better understanding the source of uncertainties. Conversely, deep learning algorithms may enable a more efficient way for scientific discovery by extracting valuable information from data and enhancing our domain expertise (Wang et al, 2023). From this perspective, deep learning and physics-based methods are not in conflict but represent a complementary approach to be jointly advanced (Levine and Tu, 2024), also in view of better quantifying and understanding the involved uncertainties.

Acronyms

AI	Artificial Intelligence
ATBD	Algorithm Theoretical Basis Document
BCNN	Bayesian Convolutional Neural Network
BDL	Bayesian Deep Learning
BLR	Bayesian Linear Regression
BNN	Bayesian Neural Network
C3S	Copernicus Climate Change Service
CNN	Convolution Neural Network
CLMS	Copernicus Land Monitoring Service
DE	Deep Ensembles
ECV	Essential Climate Variable
ELBO	Evidence Lower Bound
EO	Earth Observation
ESA CCI	European Space Agency Climate Change Initiative
EWH	Equivalent Water Height
GCOS	Global Climate Observing System
GRACE	Gravity Recovery and Climate Experiment
GRACE-FO	Gravity Recovery and Climate Experiment Follow-On
HMC	Hamiltonian Monte Carlo
KL	Kullback-Leible
LoRA	Low-rank Adaptations
LSTM	Long Short-Term Memory
MC	Monte Carlo
MC-Dropout	Monte Carlo Dropout
MCMC	Markov Chain Monte Carlo
MLE	Maximum Likelihood Estimation
MLP	Multilayer Perception
NOAA	National Oceanic and Atmospheric Administration
PINN	Physics-informed Neural Network
PODAAC	Physical Oceanography Distributed Active Archive Center
RMSE	Root Mean Squared Error
SCF	Snow Cover Fraction
SGD	Stochastic Gradient Descent
SWA	Stochastic Weight Averaging
SWAG	Stochastic Weight Averaging with a Gaussian
sEO	Satellite Earth Observation
TWS	Terrestrial Water Storage
TWSA	Terrestrial Water Storage Anomaly
TWSC	Terrestrial Water Storage Change
VI	Variational Inference
xAI	Explainable Artificial Intelligence

Declarations

Acknowledgments. This paper is an outcome of the Workshop “Remote Sensing in Climatology: Essential Climate Variables and their Uncertainties” held at the International Space Science Institute (ISSI) in Bern, Switzerland, 13-17 November 2023.

Author contributions. Conceptualization: JG, AS, BS. Data curation & Investigation: JG, AS, BS, AUW. Visualization: JG, AS. Discussion - ECV and conventional methods: JG, MJT, UM, EB, IV, AJ. Discussion - Deep learning: JG, AS, MKS, FD, KS, BS. Writing – initial draft: JG, AS, MKS, MJT, UM, EB, IV. Writing – review & editing: All authors.

Funding. AS, AUW, and FD were supported by the KnowEarth project, Norwegian Research Council (grant 337481) and the ESA project AI4Arctic.

Competing interests. The authors declare no competing interests.

Data availability. The used datasets are declared in the text with proper references. All the other intermediate data generated during this study are available from the corresponding author upon a reasonable request.

Code availability. The used open-source codes have been declared in the text. The original codes generated during this study are available from the corresponding author upon a reasonable request.

Appendix A Processing pipeline of GRACE(-FO) data and associated uncertainty sources

To explain the sources of uncertainties in a typical satellite-based parameter estimation pipeline in more details as an addition to Section 2.2.2, we further describe the multiple levels of products and their associated uncertainty propagation in a processing pipeline using the GRACE(-FO) satellite missions as an example.

Temporal variations in the mass distribution at the Earth’s surface are derived from their impacts on satellite trajectories. Therefore, one of the main observable quantities is the satellites’ absolute positions, which are determined in a precise orbit determination (POD) with centimeter accuracy from GPS code and phase observations (Jäggi et al, 2006). In the case of the dedicated gravimetry missions GRACE (Tapley et al, 2004) and GRACE-FO (Landerer et al, 2020), additional K-band and laser range (only for GRACE-FO) observations of the inter-satellite range variations of the two satellites, can be obtained with sub-micrometer per second accuracy. The inter-satellite range observations are differentiated into range rates to reduce the impact of low-frequency errors. In both cases, the GPS phase and the K-band microwave observations, the integer phase ambiguities are not observable. The processing from raw measurements (L0) to preprocessed observations (L1) is usually done by the space agency (here, JPL) and may include irreversible steps (Wen et al, 2019) and release to public for further processing. At this stage, the preliminary errors come from the inherent randomness in the measuring sensors (preliminary for L0) but also include epistemic uncertainties that come from potential model deficiencies (preliminary for L1), see Fig. 1.

The direct interpretation of L1 observations in the sense of gravity variations or mass changes is not possible and requires further complex inversion processing steps, known as L1 to L2. The data processing from L1 products to L2 products include retrieving geophysical signals from the observed data (Mittaz et al, 2019). In the case of the GRACE(-FO) missions, we need additional information to separate the impacts of the gravitational forces on the orbits of satellites from the impacts of the non-gravitational forces, such as atmospheric drag, solar radiation pressure, and Earth re-radiation. For example, the surface forces acting on the GRACE(-FO) satellites are measured by accelerometers located in the center of mass of the individual satellites, and the satellites’ attitudes are determined from star camera observations. All these observations come with observation noises, the characteristics of which is rather poorly known. Moreover, the systemic problems of the accelerometers that occurred at the final stage of GRACE, and the beginning of GRACE-FO missions also brought considerable observation uncertainties. Once the surface forces have been removed from the observations, the remaining gravitational force has to be further reduced because many mass transport processes in the Earth system happen at frequencies that are too high to be resolved by the snapshot solutions of the gravity field, which are derived at monthly intervals. This signal separation step is known as de-aliasing. It is based on models of the mass effects of the ocean, solid Earth, atmosphere tides, and the non-tidal atmosphere and ocean variations, caused mainly by weather phenomena. Again,

the tide models and the non-tidal atmosphere and ocean de-aliasing model (AOD; [Shihora et al 2022](#)) rely on observations and come with error budgets, which are not sufficiently known.

The L2 products can be further processed to generate L3 or L4 products, which are typically gridded and may include information from other geophysical data. A typical L3 product from GRACE(-FO) satellites is the gridded mass anomaly product in terms of equivalent water height ([Boergens, 2021](#); [Dahle et al, 2024](#)), whereas L4 products are further processed to generate high-level variables like global mean sea level changes or environmental extremes indicators ([Tapley et al, 2019](#)). In the processing from L2 to L3, additional geophysical background models, such as those for glacial isostatic adjustment or earthquakes, are usually applied, introducing further uncertainties ([Dahle et al, 2024](#)). Due to these diverse and poorly known sources of uncertainty, formal uncertainty propagation on the gravity field coefficients does not provide realistic results ([Boergens et al, 2022](#)). The individual analysis centers of GRACE(-FO) data developed individual approaches to absorb noise by dedicated parameters ([Beutler et al, 2010a,b](#)) or to consider it by empirical noise models ([Kvas and Mayer-Gürr, 2019](#)). Consequently, the uncertainty information provided with the gravity field solutions is also very diverse, and again, propagation of the uncertainties to mass transport products of interest for the users of the ECVs is currently not feasible.

Appendix B Sensitivity Analysis

Sensitivity analysis is another commonly used uncertainty quantification approach. By systematically investigating the relationship between input variables and model outputs, sensitivity analysis provides uncertainty quantification in complex systems ([Hofer, 1999](#); [Cacuci and Ionescu-Bujor, 2004](#)) and can be categorized into two classes:

- **Local sensitivity analysis:** Examines the impact of small changes in parameters on the output ([Gustafson et al, 1996](#)). In other words, it examines how a slight change in one input (while keeping others fixed) influences the output. Typically, this is achieved by computing partial derivatives of the output for each input parameter.
- **Global sensitivity analysis:** Considers the entire input space and assesses the contribution of each input parameter to the output variability ([Haaker and Verheijen, 2004](#)). It explores the overall contribution of each input to the variability of the model output. Instead of just looking at small local perturbations, global sensitivity analysis considers the whole range of input uncertainties and how they propagate through the model ([Chen et al, 2005](#)).

Sampling-based methods play a crucial role in both local and global sensitivity analysis, particularly in global approaches where the focus is on the entire input space. These methods involve generating samples from the input parameter space and then

propagating them through the model to observe their impact on the output ([Cacuci and Ionescu-Bujor, 2004](#)).

References

- Abadi M, Agarwal A, Barham P, et al (2015) TensorFlow: Large-Scale Machine Learning on Heterogeneous Systems. URL <https://www.tensorflow.org/>, software available from tensorflow.org
- Abdalla S, Kolahchi AA, Ablain M, et al (2021) Altimetry for the future: Building on 25 years of progress. *Advances in Space Research* 68(2):319–363. <https://doi.org/10.1016/j.asr.2021.01.022>
- Abdar M, Pourpanah F, Hussain S, et al (2021) A review of uncertainty quantification in deep learning: Techniques, applications and challenges. *Information fusion* 76:243–297. <https://doi.org/10.1016/j.inffus.2021.05.008>
- AghaKouchak A, Chiang F, Huning LS, et al (2020) Climate extremes and compound hazards in a warming world. *Annual Review of Earth and Planetary Sciences* 48(1):519–548. <https://doi.org/10.1146/annurev-earth-071719-055228>
- Altikat S (2021) Prediction of CO2 emission from greenhouse to atmosphere with artificial neural networks and deep learning neural networks. *International Journal of Environmental Science and Technology* 18:3169–3178. <https://doi.org/10.1007/s13762-020-03079-z>
- Amiri-Simkooei A, Tiberius C, Lindenbergh R (2024) Deep learning in standard least-squares theory of linear models: Perspective, development and vision. *Engineering Applications of Artificial Intelligence* 138:109376. <https://doi.org/10.1016/j.engappai.2024.109376>
- Anderson K, Ryan B, Sonntag W, et al (2017) Earth observation in service of the 2030 Agenda for Sustainable Development. *Geo-spatial Information Science* 20(2):77–96. <https://doi.org/10.1080/10095020.2017.1333230>
- Andersson T, Hosking J, Pérez-Ortiz M, et al (2021) Seasonal Arctic sea ice forecasting with probabilistic deep learning. *Nature Communications* 12(5124). <https://doi.org/10.1038/s41467-021-25257-4>
- Ansari S, Rennie C, Jamieson E, et al (2023) RivQNet: Deep Learning Based River Discharge Estimation Using Close-Range Water Surface Imagery. *Water Resources Research* 59(2):e2021WR031841. <https://doi.org/10.1029/2021WR031841>
- Ayhan MS, Berens P (2018) Test-time data augmentation for estimation of heteroscedastic aleatoric uncertainty in deep neural networks. In: *Medical Imaging with Deep Learning*
- Ballari D, Vilches-Blázquez LM, Orellana-Samaniego ML, et al (2023) Satellite Earth Observation for Essential Climate Variables Supporting Sustainable Development Goals: A Review on Applications. *Remote Sensing* 15(11):2716. <https://doi.org/10.3390/rs15112716>

- Bayat B, Camacho F, Nickeson J, et al (2021) Toward operational validation systems for global satellite-based terrestrial essential climate variables. *International Journal of Applied Earth Observation and Geoinformation* 95:102240. <https://doi.org/10.1016/j.jag.2020.102240>
- Beutler G, Jäggi A, Mervart L, et al (2010a) The celestial mechanics approach: theoretical foundations. *Journal of Geodesy* 84(10):605–624. <https://doi.org/10.1007/s00190-010-0401-7>
- Beutler G, Jäggi A, Mervart L, et al (2010b) The celestial mechanics approach: applicatin to data of the GRACE mission. *Journal of Geodesy* 84(11):661–681. <https://doi.org/10.1007/s00190-010-0402-6>
- Bi K, Xie L, Zhang H, et al (2023) Accurate medium-range global weather forecasting with 3D neural networks. *Nature* 619(7970):533–538. <https://doi.org/10.1038/s41586-023-06185-3>
- Bishop CM (2006) *Pattern recognition and machine learning*, vol 4. Springer
- Blei DM, Kucukelbir A, McAuliffe JD (2017) Variational inference: A review for statisticians. *Journal of the American statistical Association* 112(518):859–877. <https://doi.org/10.1080/01621459.2017.1285773>
- Blundell C, Cornebise J, Kavukcuoglu K, et al (2015) Weight uncertainty in neural network. In: *International conference on machine learning*, PMLR, pp 1613–1622
- Bodnar C, Bruinsma WP, Lucic A, et al (2024) Aurora: A foundation model of the atmosphere. *arXiv preprint arXiv:240513063* <https://doi.org/10.48550/arXiv.2405.13063>
- Boergens E (2021) Python Package Regional TWS Uncertainty. GFZ Data Services, <https://doi.org/10.5880/GFZ.1.3.2021.005>
- Boergens E, Kvas A, Eicker A, et al (2022) Uncertainties of GRACE-Based Terrestrial Water Storage Anomalies for Arbitrary Averaging Regions. *Journal of Geophysical Research: Solid Earth* <https://doi.org/10.1029/2021JB022081>
- Bojinski S, Verstraete M, Peterson TC, et al (2014) The concept of essential climate variables in support of climate research, applications, and policy. *Bulletin of the American Meteorological Society* 95(9):1431–1443. <https://doi.org/10.1175/BAMS-D-13-00047.1>
- Boyen X, Koller D (2013) Tractable inference for complex stochastic processes. *arXiv preprint arXiv:13017362* <https://doi.org/10.48550/arXiv.1301.7362>

- Bradbury M, Conley D (2021) Using artificial neural networks for the estimation of subsurface tidal currents from high-frequency radar surface current measurements. *Remote Sensing* 13(19):3896. <https://doi.org/10.3390/rs13193896>
- Brown RD, Robinson DA (2011) Northern Hemisphere spring snow cover variability and change over 1922–2010 including an assessment of uncertainty. *The Cryosphere* 5(1):219–229
- Buontempo C, Burgess SN, Dee D, et al (2022) The Copernicus climate change service: climate science in action. *Bulletin of the American Meteorological Society* 103(12):E2669–E2687. <https://doi.org/10.1175/BAMS-D-21-0315.1>
- Butt J, Wieser A, Gojcic Z, et al (2021) Machine learning and geodesy: A survey. *Journal of Applied Geodesy* 15(2):117–133. <https://doi.org/10.1515/jag-2020-0043>
- Cacuci DG, Ionescu-Bujor M (2004) A comparative review of sensitivity and uncertainty analysis of large-scale systems—ii: statistical methods. *Nuclear science and engineering* 147(3):204–217
- Casella G, Mengersen KL, Robert CP, et al (2002) Perfect samplers for mixtures of distributions. *Journal of the Royal Statistical Society Series B: Statistical Methodology* 64(4):777–790
- Castro-Valdecantos P, Apolo-Apolo O, Pérez-Ruiz M, et al (2022) Leaf area index estimations by deep learning models using RGB images and data fusion in maize. *Precision Agriculture* 23:1949–1966. <https://doi.org/10.1007/s11119-022-09940-0>
- Chen H, Lin X, Sun Y, et al (2023) Performance assessment of four data-driven machine learning models: a case to generate Sentinel-2 albedo at 10 meters. *Remote Sensing* 15(10):2684. <https://doi.org/10.3390/rs15102684>
- Chen W, Jin R, Sudjianto A (2005) Analytical variance-based global sensitivity analysis in simulation-based design under uncertainty. *Journal of mechanical design* 127(5):875–886
- Chen Y, Li S, Wang L, et al (2024) Retrieving freeze-thaw states using deep learning with remote sensing data in permafrost landscapes. *International Journal of Applied Earth Observation and Geoinformation* 126:103616. <https://doi.org/10.1016/j.jag.2023.103616>
- Chuvieco E (2020) *Fundamentals of satellite remote sensing: An environmental approach*. CRC press
- Ciranni M, Murino V, Odone F, et al (2024) Computer vision and deep learning meet plankton: milestones and future directions. *Image and Vision Computing* 143:104934. <https://doi.org/10.1016/j.imavis.2024.104934>

- Clare MC, Sonnewald M, Lguensat R, et al (2022) Explainable artificial intelligence for Bayesian neural networks: Toward trustworthy predictions of ocean dynamics. *Journal of Advances in Modeling Earth Systems* 14(11):e2022MS003162. <https://doi.org/10.1029/2022MS003162>
- Cobb AD, Himes MD, Soboczenski F, et al (2019) An ensemble of bayesian neural networks for exoplanetary atmospheric retrieval. *The astronomical journal* 158(1):33. <https://doi.org/10.3847/1538-3881/ab2390>
- Contractor S, Roughan M (2021) Efficacy of feedforward and LSTM neural networks at predicting and gap filling coastal ocean timeseries: oxygen, nutrients, and temperature. *Frontiers in Marine Science* 8. <https://doi.org/10.3389/fmars.2021.637759>
- Cui G, Anderson M, Bales R (2023) Mapping of snow water equivalent by a deep-learning model assimilating snow observations. *Journal of Hydrology* 616:128835. <https://doi.org/10.1016/j.jhydrol.2022.128835>
- Dahle C, Boergens E, Sasgen I, et al (2024) GravIS: Mass anomaly products from satellite gravimetry. *Earth System Science Data Discussions* pp 1–31. <https://doi.org/10.5194/essd-2024-347>
- D’Angelo F, Fortuin V (2021) Repulsive deep ensembles are Bayesian. In: *Neural Information Processing Systems (NeurIPS)*, <https://doi.org/10.48550/arXiv.2106.11642>
- Dangendorf S, Frederikse T, Chafik L, et al (2021) Data-driven reconstruction reveals large-scale ocean circulation control on coastal sea level. *Nature Climate Change* 11(6):514–520. <https://doi.org/10.1038/s41558-021-01046-1>
- Das H, H.S. D, Bhattacharjee S (2021) Forecasting upper air wind speed using a hybrid SVR-LSTM model. In: *2nd International Conference on Range Technology (ICORT)*, <https://doi.org/10.1109/ICORT52730.2021.9581478>
- De Lannoy GJM, de Rosnay P, Reichle RH (2019) Soil Moisture Data Assimilation. In: Duan Q, Pappenberger F, Wood A, et al (eds) *Handbook of Hydrometeorological Ensemble Forecasting*. Springer, Berlin, Heidelberg, p 701–743, https://doi.org/10.1007/978-3-642-39925-1_32
- Deisenroth MP, Faisal AA, Ong CS (2020) *Mathematics for machine learning*. Cambridge University Press
- Deng J, Dong W, Socher R, et al (2009) Imagenet: A large-scale hierarchical image database. In: *2009 IEEE conference on computer vision and pattern recognition*, IEEE, pp 248–255, <https://doi.org/10.1109/CVPR.2009.5206848>

- Du H, Li M, Xu Y, et al (2023) An ensemble learning approach for land use/land cover classification of arid regions for climate simulation: a case study of Xinjiang, Northwest China. *IEEE Journal of Selected Topics in Applied Earth Observations and Remote Sensing* 16:2413–2426. <https://doi.org/10.1109/JSTARS.2023.3247624>
- Eckert N, Corona C, Giacona F, et al (2024) Climate change impacts on snow avalanche activity and related risks. *Nat Rev Earth Environ* 5:369–389. <https://doi.org/10.1038/s43017-024-00540-2>
- Efron B (1979) Bootstrap methods: another look at the jackknife. *The annals of Statistics* pp 1–26
- Elachi C, Van Zyl JJ (2021) Introduction to the physics and techniques of remote sensing. John Wiley & Sons, <https://doi.org/10.1002/9781119523048>
- Folino G, Guarascio M, Chiaravalloti F (2023) Learning ensembles of deep neural networks for extreme rainfall event detection. *Neural Computing and Applications* 35:10347–10360. <https://doi.org/10.1007/s00521-023-08238-0>
- Fort S, Hu H, Lakshminarayanan B (2019) Deep ensembles: A loss landscape perspective. arXiv preprint arXiv:1912.02757 <https://doi.org/10.48550/arXiv.1912.02757>
- Fortuin V, Garriga-Alonso A, Ober SW, et al (2021) Bayesian neural network priors revisited. *ICLR 2022* <https://doi.org/10.48550/arXiv.2102.06571>
- Gal Y, Ghahramani Z (2016) Dropout as a bayesian approximation: Representing model uncertainty in deep learning. In: international conference on machine learning, PMLR, pp 1050–1059, <https://doi.org/10.48550/arXiv.1506.02142>
- Galdies C, Guerra R (2023) High resolution estimation of ocean dissolved inorganic carbon, total alkalinity and pH based on deep learning. *Water* 15(8):1454. <https://doi.org/10.3390/w15081454>
- Ganaie MA, Hu M, Malik AK, et al (2022) Ensemble deep learning: A review. *Engineering Applications of Artificial Intelligence* 115:105151. <https://doi.org/10.1016/j.engappai.2022.105151>
- Garbin C, Zhu X, Marques O (2020) Dropout vs. batch normalization: an empirical study of their impact to deep learning. *Multimedia tools and applications* 79(19):12777–12815. <https://doi.org/10.1007/s11042-019-08453-9>
- Gavahi K, Foroumandi E, Moradkhani H (2023) A deep learning-based framework for multi-source precipitation fusion. *Remote Sensing of Environment* 295:113723. <https://doi.org/10.1016/j.rse.2023.113723>
- Gawlikowski J, Tassi CRN, Ali M, et al (2023) A survey of uncertainty in deep neural networks. *Artificial Intelligence Review* 56(Suppl 1):1513–1589. <https://doi.org/10.1007/s10462-023-10453-9>

1007/s10462-023-10562-9

- George T, Manucharyan G, Thompson A (2021) Deep learning to infer eddy heat fluxes from sea surface height patterns of mesoscale turbulence. *Nature Communications* 12(800). <https://doi.org/10.1038/s41467-020-20779-9>
- Gerdener H, Kusche J, Schulze K, et al (2023) The global land water storage data set release 2 (GLWS2. 0) derived via assimilating GRACE and GRACE-FO data into a global hydrological model. *Journal of Geodesy* 97(7):73. <https://doi.org/10.1007/s00190-023-01763-9>
- Gerges F, Boufadel MC, Bou-Zeid E, et al (2024) Downscaling daily wind speed with Bayesian deep learning for climate monitoring. *International Journal of Data Science and Analytics* 17(4):411–424. <https://doi.org/10.1007/s41060-023-00397-6>
- Giroto M, Musselman KN, Essery RLH (2020) Data Assimilation Improves Estimates of Climate-Sensitive Seasonal Snow. *Current Climate Change Reports* 6(3):81–94. <https://doi.org/10.1007/s40641-020-00159-7>
- Giuliani G, Egger E, Italiano J, et al (2020) Essential variables for environmental monitoring: what are the possible contributions of earth observation data cubes? *Data* 5(4):100. <https://doi.org/10.3390/data5040100>
- Goodfellow I, Bengio Y, Courville A (2016) *Deep Learning*. MIT Press, <http://www.deeplearningbook.org>
- Goswami S, Ternikar CR, Kandala R, et al (2024) Water budget-based evapotranspiration product captures natural and human-caused variability. *Environmental Research Letters* 19(9):094034. <https://doi.org/10.1088/1748-9326/ad63bd>
- Gou J, Soja B (2024) Global high-resolution total water storage anomalies from self-supervised data assimilation using deep learning algorithms. *Nature Water* 2(2):139–150. <https://doi.org/10.1038/s44221-024-00194-w>
- Gou J, Tourian MJ (2022) RiwiSAR-SWH: A data-driven method for estimating significant wave height using Sentinel-3 SAR altimetry. *Advances in Space Research* 69(5):2061–2080. <https://doi.org/10.1016/j.asr.2021.12.019>
- Gou J, Kiani Shahvandi M, Hohensinn R, et al (2023) Ultra-short-term prediction of LOD using LSTM neural networks. *Journal of Geodesy* 97(5):52. <https://doi.org/10.1007/s00190-023-01745-x>
- Gou J, Börger L, Schindelegger M, et al (2024) Downscaling grace-derived ocean bottom pressure anomalies using self-supervised data fusion. *arXiv preprint arXiv:240405818* <https://doi.org/10.48550/arXiv.2404.05818>

- GRDC (2020) GRDC Major River Basins. Global Runoff Data Centre. 2nd, rev. ed. Koblenz: Federal Institute of Hydrology (BfG). GRDC Major River Basins of the World
- Gruber C, Schenk PO, Schierholz M, et al (2023) Sources of Uncertainty in Machine Learning—A Statisticians’ View. arXiv preprint arXiv:230516703 <https://doi.org/10.48550/arXiv.2305.16703>
- Guillou N, Chapalain G, Petton S (2023) Predicting sea surface salinity in a tidal estuary with machine learning. *Oceanologia* 65(2):318–332. <https://doi.org/10.1016/j.oceano.2022.07.007>
- Güntner A, Sharifi E, Haas J, et al (2024) Global Gravity-based Groundwater Product (G3P). <https://doi.org/10.5880/G3P.2024.001>
- Gustafson P, Srinivasan C, Wasserman L (1996) Local sensitivity analysis. *Bayesian statistics* 5:197–210
- Haaker M, Verheijen PJ (2004) Local and global sensitivity analysis for a reactor design with parameter uncertainty. *Chemical Engineering Research and Design* 82(5):591–598
- Halbheer M, Mühlematter DJ, Becker A, et al (2024) LoRA-Ensemble: Efficient Uncertainty Modelling for Self-attention Networks. arXiv preprint arXiv:240514438 <https://doi.org/10.48550/arXiv.2405.14438>
- Hall DK, Riggs GA, Salomonson VV, et al (2002) MODIS snow-cover products. *Remote sensing of Environment* 83(1-2):181–194. [https://doi.org/10.1016/S0034-4257\(02\)00095-0](https://doi.org/10.1016/S0034-4257(02)00095-0)
- Hamrani A, Akbarzadeh A, Madramootoo C (2020) Machine learning for predicting greenhouse gas emissions from agricultural soils. *Science of The Total Environment* 741:140338. <https://doi.org/10.1016/j.scitotenv.2020.140338>
- Han W, He TL, Jiang Z, et al (2023) The capability of deep learning model to predict Ozone across continents in China, the United States and Europe. *Geophysical Research Letters* 50(24):e2023GL104928. <https://doi.org/10.1029/2023GL104928>
- Haynes K, Stock J, Dostalek J, et al (2024) Exploring the use of machine learning to improve vertical profiles of temperature and moisture. *Artificial Intelligence for the Earth Systems* 3(1). <https://doi.org/10.1175/AIES-D-22-0090.1>
- He W, Jiang Z (2023) A survey on uncertainty quantification methods for deep neural networks: An uncertainty source perspective. arXiv preprint arXiv:230213425 <https://doi.org/10.48550/arXiv.2302.13425>

- Herron EJ, Young SR, Potok TE (2020) Ensembles of networks produced from neural architecture search. In: International Conference on High Performance Computing, Springer, pp 223–234. https://doi.org/10.1007/978-3-030-59851-8_14
- Heydari S, Nikoo M, Mohammadi A, et al (2024) Two-stage meta-ensembling machine learning model for enhanced water quality forecasting. *Journal of Hydrology* 641. <https://doi.org/10.1016/j.jhydrol.2024.131767>
- Ho J, Jain A, Abbeel P (2020) Denoising diffusion probabilistic models. *Advances in neural information processing systems* 33:6840–6851. <https://doi.org/10.48550/arXiv.2006.11239>
- Hofer E (1999) Sensitivity analysis in the context of uncertainty analysis for computationally intensive models. *Computer Physics Communications* 117(1-2):21–34
- Hoffmann D, Gallant AJE, Arblaster JM (2020) Uncertainties in Drought From Index and Data Selection. *Journal of Geophysical Research: Atmospheres* 125(18):e2019JD031946. <https://doi.org/10.1029/2019JD031946>
- Hora SC (1996) Aleatory and epistemic uncertainty in probability elicitation with an example from hazardous waste management. *Reliability Engineering & System Safety* 54(2-3):217–223. [https://doi.org/10.1016/S0951-8320\(96\)00077-4](https://doi.org/10.1016/S0951-8320(96)00077-4)
- Hornik K, Stinchcombe M, White H (1989) Multilayer feedforward networks are universal approximators. *Neural networks* 2(5):359–366. [https://doi.org/10.1016/0893-6080\(89\)90020-8](https://doi.org/10.1016/0893-6080(89)90020-8)
- Humphrey GB, Gibbs MS, Dandy GC, et al (2016a) A hybrid approach to monthly streamflow forecasting: integrating hydrological model outputs into a Bayesian artificial neural network. *Journal of Hydrology* 540:623–640. <https://doi.org/10.1016/j.jhydrol.2016.06.026>
- Humphrey V, Gudmundsson L, Seneviratne SI (2016b) Assessing global water storage variability from GRACE: Trends, seasonal cycle, subseasonal anomalies and extremes. *Surveys in geophysics* 37:357–395. <https://doi.org/10.1007/s10712-016-9367-1>
- Hüsler F, Jonas T, Riffler M, et al (2014) A satellite-based snow cover climatology (1985–2011) for the European Alps derived from AVHRR data. *The Cryosphere* 8(1):73–90
- Izmailov P, Podoprikin D, Garipov T, et al (2018) Averaging weights leads to wider optima and better generalization. arXiv preprint arXiv:180305407 <https://doi.org/10.48550/arXiv.1803.05407>
- Izmailov P, Vikram S, Hoffman MD, et al (2021) What are Bayesian neural network posteriors really like? In: International conference on machine learning, PMLR, pp

- Jagannathan J, Divya C (2021) Deep learning for the prediction and classification of land use and land cover changes using deep convolutional neural network. *Ecological Informatics* 65:101412. <https://doi.org/10.1016/j.ecoinf.2021.101412>
- Jäggi A, Beutler G, Bock H, et al (2006) Kinematic and highly reduced-dynamic LEO orbit determination for gravity field estimation. In: Rizos C, Tregoning P (eds) *Dynamic Planet - Monitoring and Understanding a Dynamic Planet with Geodetic and Oceanographic Tools*. Springer, p 354–361
- Jana RB, Mohanty BP, Springer EP (2008) Multiscale Bayesian neural networks for soil water content estimation. *Water Resources Research* 44(8). <https://doi.org/10.1029/2008WR006879>
- Jeppesen JH, Jacobsen RH, Inceoglu F, et al (2019) A cloud detection algorithm for satellite imagery based on deep learning. *Remote sensing of environment* 229:247–259. <https://doi.org/10.1016/j.rse.2019.03.039>
- Jiang S, Sweet Lb, Blougouras G, et al (2024a) How Interpretable Machine Learning Can Benefit Process Understanding in the Geosciences. *Earth's Future* 12(7):e2024EF004540. <https://doi.org/10.1029/2024EF004540>
- Jiang W, Liu B, Liang Y, et al (2024b) Applicability analysis of transformer to wind speed forecasting by a novel deep learning framework with multiple atmospheric variables. *Applied Energy* 353(B):122155. <https://doi.org/10.1016/j.apenergy.2023.122155>
- Jose D, Vincent A, Dwarakish G (2022) Improving multiple model ensemble predictions of daily precipitation and temperature through machine learning techniques. *Scientific Reports* 12(4678). <https://doi.org/10.1038/s41598-022-08786-w>
- Jospin LV, Laga H, Boussaid F, et al (2022) Hands-on Bayesian neural networks—A tutorial for deep learning users. *IEEE Computational Intelligence Magazine* 17(2):29–48. <https://doi.org/10.1109/MCI.2022.3155327>
- Jungmann P, Poray J, Kumar A (2024) Analytical uncertainty propagation in neural networks. *IEEE Transactions on Neural Networks and Learning Systems* <https://doi.org/10.1109/TNNLS.2023.3347156>
- Kahl KC, Lüth CT, Zenk M, et al (2024) A framework for systematic validation of uncertainty estimation in semantic segmentation. arXiv preprint arXiv:240108501 URL <https://arxiv.org/abs/2401.08501>
- Kang X, Kokkinaki A, Shi X, et al (2024) Modeling upscaled mass discharge from complex DNAPL source zones using a Bayesian neural network: Prediction accuracy, uncertainty quantification and source zone feature importance. *Water Resources*

- Research 60(7):e2023WR036864. <https://doi.org/10.1029/2023WR036864>
- Karmakar S, Roy S, Kar A, et al (2023) Deep neural net based approach for air pressure prediction. In: Second International Conference on Innovations in Software Architecture and Computational Systems, <https://doi.org/10.1063/5.0166718>
- Kendall A, Gal Y (2017) What uncertainties do we need in bayesian deep learning for computer vision? *Advances in neural information processing systems* 30
- Khalaf G, Shukur G (2005) Choosing ridge parameter for regression problems. *Communications in Statistics - Theory and Methods* <https://doi.org/10.1081/STA-200056836>
- Khan MS, Coulibaly P (2006) Bayesian neural network for rainfall-runoff modeling. *Water Resources Research* 42(7). <https://doi.org/10.1029/2005WR003971>
- Kiani Shahvandi M, Soja B (2022) Inclusion of data uncertainty in machine learning and its application in geodetic data science, with case studies for the prediction of Earth orientation parameters and GNSS station coordinate time series. *Advances in Space Research* 70(3):563–575. <https://doi.org/10.1016/j.asr.2022.05.042>
- Kiani Shahvandi M, Adhikari S, Dumberry M, et al (2024a) Contributions of core, mantle and climatological processes to Earth’s polar motion. *Nature Geoscience* 17(7). <https://doi.org/10.1038/s41561-024-01478-2>
- Kiani Shahvandi M, Belda S, Mishra S, et al (2024b) Short-term prediction of celestial pole offsets with interpretable machine learning. *Earth, Planets and Space* 76(18). <https://doi.org/10.1186/s40623-024-01964-2>
- Kiani Shahvandi M, Mishra S, Soja B (2024c) BaHaMAs: a method for uncertainty quantification in geodetic time series and its application in short-term prediction of length of day. *Earth, Planets and Space* 76(127). <https://doi.org/10.1186/s40623-024-02066-9>
- Kiani Shahvandi M, Mishra S, Soja B (2025) Laplacian deep ensembles: Methodology and application in predicting dUT1 considering geophysical fluids. *Computers & Geosciences* 196:105818. <https://doi.org/10.1016/j.cageo.2024.105818>
- Kingma DP, Ba J (2014) Adam: A method for stochastic optimization. arXiv preprint arXiv:14126980 <https://doi.org/https://doi.org/10.48550/arXiv.1412.6980>
- Kingma DP, Salimans T, Welling M (2015) Variational dropout and the local reparameterization trick. *Advances in neural information processing systems* 28
- Kingston GB, Lambert MF, Maier HR (2005) Bayesian training of artificial neural networks used for water resources modeling. *Water resources research* 41(12). <https://doi.org/10.1029/2005WR004152>

- Klein AG, Hall DK, Riggs GA (1998) Improving snow cover mapping in forests through the use of a canopy reflectance model. *Hydrological Processes*, 12(10-11):1723–1744
- Koch KR (2013) *Parameter estimation and hypothesis testing in linear models*. Springer Science & Business Media
- Kolluru S, Tiwari S (2022) Modeling ocean surface chlorophyll-a concentration from ocean color remote sensing reflectance in global waters using machine learning. *Science of The Total Environment* 844:157191. <https://doi.org/10.1016/j.scitotenv.2022.157191>
- Koppa A, Rains D, Hulsman P, et al (2022) A deep learning-based hybrid model of global terrestrial evaporation. *Nature Communications* 13(1912). <https://doi.org/10.1038/s41467-022-29543-7>
- Krause A (2022) *Probabilistic Artificial Intelligence*. ETH Zurich
- Kristiadi A, Hein M, Hennig P (2020) Being bayesian, even just a bit, fixes overconfidence in relu networks. In: *International conference on machine learning*, PMLR, pp 5436–5446
- Kuleshov V, Fenner N, Ermon S (2018) Accurate uncertainties for deep learning using calibrated regression. In: *International conference on machine learning*, PMLR, pp 2796–2804
- Kullback S, Leibler RA (1951) On information and sufficiency. *The annals of mathematical statistics* 22(1):79–86
- Kutz JN (2023) Machine learning for parameter estimation. *Proceedings of the National Academy of Sciences* 120(12):e2300990120. <https://doi.org/10.1073/pnas.2300990120>
- Kvas A, Mayer-Gürr T (2019) GRACE gravity field recovery with background model uncertainties. *Journal of Geodesy* 93(12):2543–2552. <https://doi.org/10.1007/s00190-019-01314-1>
- Laimighofer J, Laaha G (2022) How standard are standardized drought indices? Uncertainty components for the SPI & SPEI case. *Journal of Hydrology* 613:128385. <https://doi.org/10.1016/j.jhydrol.2022.128385>
- Lakshminarayanan B, Pritzel A, Blundell C (2017) Simple and scalable predictive uncertainty estimation using deep ensembles. *Advances in neural information processing systems* 30
- Lam R, Sanchez-Gonzalez A, Willson M, et al (2023) Learning skillful medium-range global weather forecasting. *Science* 382(6677):1416–1421. <https://doi.org/10.1126/science.adi2336>

- Landerer F, Flechtner F, Save H, et al (2020) Extending the global mass change data record: GRACE follow-on instrument and science data performance. *Geophys Res Lett* 47:e2020GL088306. <https://doi.org/10.1029/2020GL088306>
- Landerer FW, Dickey JO, Güntner A (2010) Terrestrial water budget of the Eurasian pan-Arctic from GRACE satellite measurements during 2003–2009. *Journal of Geophysical Research: Atmospheres* 115(D23). <https://doi.org/10.1029/2010JD014584>
- LeCun Y, Bengio Y, Hinton G (2015) Deep learning. *nature* 521(7553):436–444. <https://doi.org/10.1038/nature1453>
- Lee S, Kim H, Lee J (2022) Graddiv: Adversarial robustness of randomized neural networks via gradient diversity regularization. *IEEE Transactions on Pattern Analysis and Machine Intelligence* <https://doi.org/10.1109/TPAMI.2022.3169217>
- Lehmann EL, Romano JP (2005) *Testing Statistical Hypotheses*. Springer Science & Business Media
- Lehmann F, Vishwakarma BD, Bamber J (2022) How well are we able to close the water budget at the global scale? *Hydrology and Earth System Sciences* 26(1):35–54. <https://doi.org/10.5194/hess-26-35-2022>
- Levine H, Tu Y (2024) Machine learning meets physics: A two-way street. <https://doi.org/10.1073/pnas.2403580121>
- Li D, Marshall L, Liang Z, et al (2022a) Hydrologic multi-model ensemble predictions using variational Bayesian deep learning. *Journal of Hydrology* 604:127221. <https://doi.org/10.1016/j.jhydrol.2021.127221>
- Li S, Jiang B, Liang S, et al (2022b) Evaluation of nine machine learning methods for estimating daily land surface radiation budget from MODIS satellite data. *International Journal of Digital Earth* 15(1):1784–1816. <https://doi.org/10.1080/17538947.2022.2130460>
- Li W, Gao X, Hao Z, et al (2022c) Using deep learning for precipitation forecasting based on spatio-temporal information: a case study. *Climate Dynamics* 58(1):443–457. <https://doi.org/10.1007/s00382-021-05916-4>
- Li X, Feng M, Ran Y, et al (2023) Big Data in Earth system science and progress towards a digital twin. *Nature Reviews Earth & Environment* 4(5):319–332. <https://doi.org/10.1038/s43017-023-00409-w>
- Liang F, Wong WH (2001) Real-parameter evolutionary Monte Carlo with applications to Bayesian mixture models. *Journal of the American Statistical Association* 96(454):653–666. <https://doi.org/10.1198/016214501753168325>

- Liu G, Shih KJ, Wang TC, et al (2018) Partial convolution based padding. arXiv preprint arXiv:181111718 <https://doi.org/10.48550/arXiv.1811.11718>
- Liu G, Wang Y, Qin H, et al (2023) Probabilistic spatiotemporal forecasting of wind speed based on multi-network deep ensembles method. *Renewable Energy* 209:231–247. <https://doi.org/10.1016/j.renene.2023.03.094>
- Liu Q, Wang D (2016) Stein variational gradient descent: A general purpose bayesian inference algorithm. *Advances in neural information processing systems* 29. <https://doi.org/10.48550/arXiv.1608.04471>
- Liu Q, Kampffmeyer M, Jenssen R, et al (2020) Dense dilated convolutions' merging network for land cover classification. *IEEE Transactions on Geoscience and Remote Sensing* 58(9):6309–6320. <https://doi.org/10.1109/TGRS.2020.2976658>
- López-Puigdollers D, Mateo-García G, Gómez-Chova L (2021) Benchmarking deep learning models for cloud detection in Landsat-8 and Sentinel-2 images. *Remote Sensing* 13(5):992. <https://doi.org/10.3390/rs13050992>
- Loquercio A, Segu M, Scaramuzza D (2020) A general framework for uncertainty estimation in deep learning. *IEEE Robotics and Automation Letters* 5(2):3153–3160. <https://doi.org/10.1109/LRA.2020.2974682>
- Lu D, Liu Y, Zhang Z, et al (2024) A diffusion-based uncertainty quantification method to advance E3SM land model calibration. *Journal of Geophysical Research: Machine Learning and Computation* 1(3):e2024JH000234. <https://doi.org/10.1029/2024JH000234>
- Luo H, Yang Q, Mazloff M, et al (2023) The Impacts of Optimizing Model-Dependent Parameters on the Antarctic Sea Ice Data Assimilation. *Geophysical Research Letters* 50(22):e2023GL105690. <https://doi.org/10.1029/2023GL105690>
- Luo X, Nadiga BT, Park JH, et al (2022) A Bayesian Deep Learning Approach to Near-Term Climate Prediction. *Journal of Advances in Modeling Earth Systems* 14(10):e2022MS003058. <https://doi.org/10.1029/2022MS003058>
- Ma H, Liang S, Xiong C, et al (2022) Global land surface 250 m 8 d fraction of absorbed photosynthetically active radiation (FAPAR) product from 2000 to 2021. *Earth System Science Data* 14(12):5333–5347. <https://doi.org/10.5194/essd-14-5333-2022>
- MacKay DJC (1992) A Practical Bayesian Framework for Backpropagation Networks. *Neural Computation* 4(3):448–472. <https://doi.org/10.1162/neco.1992.4.3.448>
- Maddox WJ, Izmailov P, Garipov T, et al (2019) A simple baseline for bayesian uncertainty in deep learning. *Advances in neural information processing systems* 32

- Maiti S, Tiwari R (2014) A comparative study of artificial neural networks, Bayesian neural networks and adaptive neuro-fuzzy inference system in groundwater level prediction. *Environmental earth sciences* 71:3147–3160. <https://doi.org/10.1007/s12665-013-2702-7>
- Malakouti S (2023) Utilizing time series data from 1961 to 2019 recorded around the world and machine learning to create a global temperature change prediction model. *Case Studies in Chemical and Environmental Engineering* 7. <https://doi.org/10.1016/j.cscee.2023.100312>
- Martin S (2014) *An introduction to ocean remote sensing*. Cambridge University Press, <https://doi.org/10.1017/CBO9781139094368>
- Metsämäki S, Mattila OP, Pulliainen J, et al (2012) An optical reflectance model-based method for fractional snow cover mapping applicable to continental scale. *Remote Sensing Environ* 123:508–521
- Metsämäki S, Pulliainen J, Salminen KM, and Luojus, et al (2015) Introduction to GlobSnow Snow Extent products with considerations for accuracy assessment. *Remote Sensing Environ* 156:96–108
- Miranda Espinosa MT, Giuliani G, Ray N (2020) Reviewing the discoverability and accessibility to data and information products linked to essential climate variables. *International Journal of Digital Earth* 13(2):236–252. <https://doi.org/10.1080/17538947.2019.1620882>
- Miro ME, Famiglietti JS (2018) Downscaling GRACE remote sensing datasets to high-resolution groundwater storage change maps of California’s Central Valley. *Remote Sensing* 10(1):143. <https://doi.org/10.3390/rs10010143>
- Mittaz J, Merchant CJ, Woolliams ER (2019) Applying principles of metrology to historical earth observations from satellites. *Metrologia* 56(3):032002. <https://doi.org/10.1088/1681-7575/ab1705>
- Mittendorf M, Nielsen U, Bingham H, et al (2022) Sea state identification using machine learning—a comparative study based on in-service data from a container vessel. *Marine Structures* 85:103274. <https://doi.org/10.1016/j.marstruc.2022.103274>
- Mo S, Zhong Y, Forootan E, et al (2022) Bayesian convolutional neural networks for predicting the terrestrial water storage anomalies during GRACE and GRACE-FO gap. *Journal of Hydrology* 604:127244. <https://doi.org/10.1016/j.jhydrol.2021.127244>
- Moradi R, Berangi R, Minaei B (2020) A survey of regularization strategies for deep models. *Artificial Intelligence Review* 53(6):3947–3986. <https://doi.org/10.1007/s10462-019-09784-7>

- Mullen AL, Watts JD, Rogers BM, et al (2023) Using High-Resolution Satellite Imagery and Deep Learning to Track Dynamic Seasonality in Small Water Bodies. *Geophysical Research Letters* 50(7):e2022GL102327. <https://doi.org/10.1029/2022GL102327>
- Nair DS, Hochgeschwender N, Olivares-Mendez MA (2022) Maximum likelihood uncertainty estimation: Robustness to outliers. arXiv preprint arXiv:220203870 <https://doi.org/10.48550/arXiv.2202.03870>
- Natras R, Soja B, Schmidt M (2022) Ensemble machine learning of random forest, adaboost and xgboost for vertical total electron content forecasting. *Remote Sensing* 14(15):3547. <https://doi.org/10.3390/rs14153547>
- Neal RM (1992) Bayesian training of backpropagation networks by the hybrid monte carlo method. Tech. rep., Citeseer
- Neal RM (2011) MCMC using Hamiltonian dynamics. In: *Handbook of Markov Chain Monte Carlo*. CRC Press, p 113–162
- Neyman J, Pearson ES (1933) On the problem of the most efficient tests of statistical hypotheses. *Philosophical Transactions of the Royal Society of London Series A, Containing Papers of a Mathematical or Physical Character* 231:289–337
- Nieves V, Radin C, Camps-Valls G (2021) Predicting regional coastal sea level changes with machine learning. *Scientific Reports* 11(7650). <https://doi.org/10.1038/s41598-021-87460-z>
- Ovadia Y, Fertig E, Ren J, et al (2019) Can you trust your model’s uncertainty? evaluating predictive uncertainty under dataset shift. *Adv Neural Inform Process Syst* 32
- Paszke A, Gross S, Massa F, et al (2019) Pytorch: An imperative style, high-performance deep learning library. *Advances in neural information processing systems* 32. <https://doi.org/10.48550/arXiv.1912.01703>
- Plummer S, Lecomte P, Doherty M (2017) The ESA climate change initiative (CCI): A European contribution to the generation of the global climate observing system. *Remote Sensing of Environment* 203:2–8. <https://doi.org/10.1016/j.rse.2017.07.014>
- Povey A, Grainger R (2015a) Known and unknown unknowns: uncertainty estimation in satellite remote sensing. *Atmospheric Measurement Techniques* 8(11):4699–4718. <https://doi.org/10.5194/amt-8-4699-2015>
- Povey A, Grainger R (2015b) Known and unknown unknowns: uncertainty estimation in satellite remote sensing. *Atmospheric Measurement Techniques* 8(11):4699–4718. <https://doi.org/10.5194/amt-8-4699-2015>

- Price I, Sanchez-Gonzalez A, Alet F, et al (2023) Gencast: Diffusion-based ensemble forecasting for medium-range weather. arXiv preprint arXiv:231215796 <https://doi.org/10.48550/arXiv.2312.15796>
- Pulliainen J, Luojus K, Derksen C, et al (2020) Patterns and trends of Northern Hemisphere snow mass from 1980 to 2018. *Nature* 581(7808):294–298
- Raissi M, Perdikaris P, Karniadakis GE (2019) Physics-informed neural networks: A deep learning framework for solving forward and inverse problems involving non-linear partial differential equations. *Journal of Computational physics* 378:686–707. <https://doi.org/10.1016/j.jcp.2018.10.045>
- Rateb A, Sun A, Scanlon BR, et al (2022) Reconstruction of GRACE mass change time series using a Bayesian framework. *Earth and Space Science* 9(7):e2021EA002162. <https://doi.org/10.1029/2021EA002162>
- Reichstein M, Camps-Valls G, Stevens B, et al (2019) Deep learning and process understanding for data-driven Earth system science. *Nature* 566(7743):195–204. <https://doi.org/10.1038/s41586-019-0912-1>
- Reilly J, Stone PH, Forest CE, et al (2001) Uncertainty and climate change assessments. <https://doi.org/10.1126/science.1062001>
- Rodell M, Li B (2023) Changing intensity of hydroclimatic extreme events revealed by GRACE and GRACE-FO. *Nature Water* 1(3):241–248. <https://doi.org/10.1038/s44221-023-00040-5>
- Rolf E, Klemmer K, Robinson C, et al (2024) Mission Critical–Satellite Data is a Distinct Modality in Machine Learning. arXiv preprint arXiv:240201444 <https://doi.org/10.48550/arXiv.2402.01444>
- Ronneberger O, Fischer P, Brox T (2015) U-Net: Convolutional networks for biomedical image segmentation. In: *Int. Conf. Medical image computing and computer-assisted intervention*. p 234–241
- Roscher R, Bohn B, Duarte MF, et al (2020) Explainable machine learning for scientific insights and discoveries. *Ieee Access* 8:42200–42216. <https://doi.org/10.1109/ACCESS.2020.2976199>
- Rubbens P, Brodie S, Cordier T, et al (2023) Machine learning in marine ecology: an overview of techniques and applications. *ICES Journal of Marine Science* 80(7):1829–1853. <https://doi.org/10.1093/icesjms/fsad100>
- Saemian P, Tourian MJ, Elmi O, et al (2024) A probabilistic approach to characterizing drought using satellite gravimetry. *Water Resources Research* 60(8):e2023WR036873. <https://doi.org/10.1029/2023WR036873>

- Salminen M, Pulliainen J, Metsämäki S, et al (2018) Determination of uncertainty characteristics for the satellite data-based estimation of fractional snow cover. *Remote Sensing Environ* 212:103–113
- Samek W, Montavon G, Lapuschkin S, et al (2021) Explaining deep neural networks and beyond: A review of methods and applications. *Proceedings of the IEEE* 109(3):247–278. <https://doi.org/10.1109/JPROC.2021.3060483>
- Sathishkumar V, Cho J, Subramanian M, et al (2023) Forest fire and smoke detection using deep learning-based learning without forgetting. *Fire Ecology* 19(9). <https://doi.org/10.1186/s42408-022-00165-0>
- Schneider T, Behera S, Boccaletti G, et al (2023) Harnessing AI and computing to advance climate modelling and prediction. *Nature Climate Change* 13(9):887–889. <https://doi.org/10.1038/s41558-023-01769-3>
- Schumacher M, Kusche J, Döll P (2016) A systematic impact assessment of GRACE error correlation on data assimilation in hydrological models. *Journal of Geodesy* 90(6):537–559. <https://doi.org/10.1007/s00190-016-0892-y>
- Segal-Rozenhaimer M, Li A, Das K, et al (2020) Cloud detection algorithm for multi-modal satellite imagery using convolutional neural-networks (cnn). *Remote Sensing of Environment* 237:111446. <https://doi.org/10.1016/j.rse.2019.111446>
- Sengupta U, Amos M, Hosking S, et al (2020) Ensembling geophysical models with Bayesian neural networks. *Advances in Neural Information Processing Systems* 33:1205–1217
- Sha Y, Sobash R, Gagne D (2024) Generative ensemble deep learning severe weather prediction from a deterministic convection-allowing model. *Artificial Intelligence for the Earth Systems* 3(2):e230094. <https://doi.org/10.1175/AIES-D-23-0094.1>
- Sharp J, Fassbender A, Carter B, et al (2023) GOBAI-O2: temporally and spatially resolved fields of ocean interior dissolved oxygen over nearly 2 decades. *Earth System Science Data* 15(10):4481–4518. <https://doi.org/10.5194/essd-15-4481-2023>
- Shen H, Jiang Y, Li T, et al (2020) Deep learning-based air temperature mapping by fusing remote sensing, station, simulation and socioeconomic data. *Remote Sensing of Environment* 240:111692. <https://doi.org/10.1016/j.rse.2020.111692>
- Shihora L, Balidakis K, Dill R, et al (2022) Non-tidal background modeling for satellite gravimetry based on operational ECWMF and ERA5 reanalysis data: AOD1B RL07. *Journal of Geophysical Research: Solid Earth* 127(8):e2022JB024360. <https://doi.org/10.1029/2022JB024360>
- Singh A, Gaurav K (2023) Deep learning and data fusion to estimate surface soil moisture from multi-sensor satellite images. *Scientific Reports* 13(2251). <https://doi.org/10.1038/s41598-023-22511-1>

doi.org/10.1038/s41598-023-28939-9

- Sinha A, Abernathey R (2021) Estimating ocean surface currents with machine learning. *Frontiers in Marine Science* 8. <https://doi.org/10.3389/fmars.2021.672477>
- Smith LA, Stern N (2011) Uncertainty in science and its role in climate policy. *Philosophical Transactions of the Royal Society A: Mathematical, Physical and Engineering Sciences* 369(1956):4818–4841. <https://doi.org/10.1098/rsta.2011.0149>
- Solberg R, Salberg AB, Waldeland AU, et al (2021) Final Report: AI4Arctic Deliverable 6. Tech. rep., NR Note SAMBA/19/21, Norwegian Computing Center
- Soltani SS, Ataie-Ashtiani B, Simmons CT (2021) Review of assimilating GRACE terrestrial water storage data into hydrological models: Advances, challenges and opportunities. *Earth-Science Reviews* 213:103487. <https://doi.org/10.1016/j.earscirev.2020.103487>
- Springer A, Lopez T, Owor M, et al (2023) The role of space-based observations for groundwater resource monitoring over Africa. *Surveys in Geophysics* 44(1):123–172. <https://doi.org/10.1007/s10712-022-09759-4>
- Srivastava N, Hinton G, Krizhevsky A, et al (2014) Dropout: a simple way to prevent neural networks from overfitting. *The journal of machine learning research* 15(1):1929–1958
- Sturm M, Holmgren J, McFadden JP, et al (2001) Snow–shrub interactions in Arctic tundra: a hypothesis with climatic implications. *J Climate* 14(3):336–344. <https://doi.org/10.1002/2017WR020840>
- Sturm M, Goldstein MA, Parr C (2017) Water and life from snow: a trillion dollar science question. *Water Resour Res* 53(5):3534–3544. <https://doi.org/10.1002/2017WR020840>
- Su H, Jiang J, Wang A, et al (2022) Subsurface temperature reconstruction for the global ocean from 1993 to 2020 using satellite observations and deep learning. *Remote Sensing* 14(13):3198. <https://doi.org/10.3390/rs14133198>
- Sun H, Shin YM, Xia M, et al (2021) Spatial resolved surface ozone with urban and rural differentiation during 1990–2019: a space–time bayesian neural network downscaler. *Environmental Science & Technology* 56(11):7337–7349. <https://doi.org/10.1021/acs.est.1c04797>
- Tao C, Peng Y, Zhang Q, et al (2024) Diagnosing ozone–NO_x–VOC–aerosol sensitivity and uncovering causes of urban–nonurban discrepancies in Shandong, China, using transformer-based estimations. *Atmospheric Chemistry and Physics* 24(7):4177–4192. <https://doi.org/10.5194/acp-24-4177-2024>

- Tao M, Chen J, Xu X, et al (2023) A robust and flexible satellite aerosol retrieval algorithm for multi-angle polarimetric measurements with physics-informed deep learning method. *Remote Sensing of Environment* 297:113763. <https://doi.org/10.1016/j.rse.2023.113763>
- Tapley B, Bettadpur S, Watkins M, et al (2004) The gravity recovery and climate experiment: mission overview and early results. *Geophys Res Lett* 31:L09607. <https://doi.org/10.1029/2004GL019920>
- Tapley BD, Watkins MM, Flechtner F, et al (2019) Contributions of GRACE to understanding climate change. *Nature climate change* 9(5):358–369. <https://doi.org/10.1038/s41558-019-0456-2>
- Tarek M, Brissette F, Arsenault R (2021) Uncertainty of gridded precipitation and temperature reference datasets in climate change impact studies. *Hydrology and Earth System Sciences* 25(6):3331–3350. <https://doi.org/10.5194/hess-25-3331-2021>
- Teunissen PJ (2006) *Testing theory*. VSSD Delft
- Teunissen PJ (2024) *Adjustment theory: an introduction*. TU Delft OPEN Publishing
- Thomas D, Robson B, Racoviteanu A (2023) An integrated deep learning and object-based image analysis approach for mapping debris-covered glaciers. *Frontiers in Remote Sensing* 4. <https://doi.org/10.3389/frsen.2023.1161530>
- Tian T, Cheng L, Wang G, et al (2022) Reconstructing ocean subsurface salinity at high resolution using a machine learning approach. *Earth System Science Data* 14(11):5037–5060. <https://doi.org/10.5194/essd-14-5037-2022>
- Tian Y, Zhang Y (2022) A comprehensive survey on regularization strategies in machine learning. *Information Fusion* 80:146–166. <https://doi.org/10.1016/j.inffus.2021.11.005>
- Tollenaar V, Zekollari H, Pattyn F, et al (2024) Where the white continent is blue: deep learning locates bare ice in Antarctica. *Geophysical Research Letters* 51(3):e2023GL106285. <https://doi.org/10.1029/2023GL106285>
- Toth C, Józkó G (2016) Remote sensing platforms and sensors: A survey. *ISPRS Journal of Photogrammetry and Remote Sensing* 115:22–36. <https://doi.org/10.1016/j.isprsjprs.2015.10.004>
- Tourian MJ, Saemian P, Ferreira VG, et al (2023) A copula-supported Bayesian framework for spatial downscaling of GRACE-derived terrestrial water storage flux. *Remote Sensing of Environment* 295:113685. <https://doi.org/10.1016/j.rse.2023.113685>

- Tsai YLS, Dietz A, Oppelt N, et al (2019) Remote sensing of snow cover using space-borne SAR: A review. *Remote Sensing*. *Remote Sensing* 11(12). <https://doi.org/10.3390/rs11121456>
- Tuia D, Schindler K, Demir B, et al (2024) Artificial intelligence to advance Earth observation: A review of models, recent trends, and pathways forward. *IEEE Geoscience and Remote Sensing Magazine* <https://doi.org/10.1109/MGRS.2024.3425961>
- Turkoglu MO, Becker A, Gündüz HA, et al (2022) Film-ensemble: Probabilistic deep learning via feature-wise linear modulation. *Advances in neural information processing systems* 35:22229–22242
- Uz M, Atman KG, Akyilmaz O, et al (2022) Bridging the gap between grace and grace-fo missions with deep learning aided water storage simulations. *Science of the Total Environment* 830:154701. <https://doi.org/10.1016/j.scitotenv.2022.154701>
- Uz M, Akyilmaz O, Shum C (2024) Deep learning-aided temporal downscaling of GRACE-derived terrestrial water storage anomalies across the Contiguous United States. *Journal of Hydrology* p 132194. <https://doi.org/10.1016/j.jhydrol.2024.132194>
- Wang G, Li W, Aertsen M, et al (2019) Aleatoric uncertainty estimation with test-time augmentation for medical image segmentation with convolutional neural networks. *Neurocomputing* 338:34–45. <https://doi.org/https://doi.org/10.1016/j.neucom.2019.01.103>
- Wang H, Mao K, Yuan Z, et al (2021) A method for land surface temperature retrieval based on model-data-knowledge-driven and deep learning. *Remote Sensing of Environment* 265:112665. <https://doi.org/10.1016/j.rse.2021.112665>
- Wang H, Fu T, Du Y, et al (2023) Scientific discovery in the age of artificial intelligence. *Nature* 620(7972):47–60. <https://doi.org/10.1038/s41586-023-06221-2>
- Wen H, Kruizinga G, Paik M, et al (2019) Gravity Recovery and Climate Experiment Follow-On (GRACE-FO) Level-1 Data Product User Handbook. URL <https://podaac.jpl.nasa.gov/gravity/gracefo-documentation>
- Wilson AG, Izmailov P (2020) Bayesian deep learning and a probabilistic perspective of generalization. *Advances in neural information processing systems* 33:4697–4708
- Wright N, Duncan J, Callow J, et al (2024) CloudS2Mask: a novel deep learning approach for improved cloud and cloud shadow masking in Sentinel-2 imagery. *Remote Sensing of Environment* 306:114122. <https://doi.org/10.1016/j.rse.2024.114122>

- Wu Y, Jiang N, Xu Y, et al (2023) Improving the capability of water vapor retrieval from Landsat 8 using ensemble machine learning. *International Journal of Applied Earth Observation and Geoinformation* 122:103407. <https://doi.org/10.1016/j.jag.2023.103407>
- Wunsch A, Liesch T, Broda S (2022) Deep learning shows declining groundwater levels in Germany until 2100 due to climate change. *Nature Communications* 13(1221). <https://doi.org/10.1038/s41467-022-28770-2>
- Wylie BK, Fosnight EA, Gilmanov TG, et al (2007) Adaptive data-driven models for estimating carbon fluxes in the Northern Great Plains. *Remote Sensing of Environment* 106(4):399–413. <https://doi.org/10.1016/j.rse.2006.09.017>
- Xiao C, Chen N, Hu C, et al (2019) Short and mid-term sea surface temperature prediction using time-series satellite data and LSTM-AdaBoost combination approach. *Remote Sensing of Environment* 233:111358. <https://doi.org/10.1016/j.rse.2019.111358>
- Xu L, Chen N, Yang C (2021) Quantifying the uncertainty of precipitation forecasting using probabilistic deep learning. *Hydrology and Earth System Sciences Discussions* 2021:1–27. <https://doi.org/10.5194/hess-26-2923-2022>
- Yan H, Sun N, Wigmosta MS, et al (2023) The role of snowmelt temporal pattern in flood estimation for a small snow-dominated basin in the sierra nevada. *Water Resources Research* 59. <https://doi.org/10.1029/2023WR034496>
- Yang L, Cai Y, Zhang L, et al (2021) A deep learning method to predict soil organic carbon content at a regional scale using satellite-based phenology variables. *International Journal of Applied Earth Observation and Geoinformation* 102:102428. <https://doi.org/10.1016/j.jag.2021.102428>
- Yang S, Chang B, Warner M, et al (2020) Global reconstruction reduces the uncertainty of oceanic nitrous oxide emissions and reveals a vigorous seasonal cycle. *Proceedings of the National Academy of Sciences* 117(22):11954–11960. <https://doi.org/10.1073/pnas.1921914117>
- Yao Y, Zhong X, Zheng Y, et al (2023) A physics-incorporated deep learning framework for parameterization of atmospheric radiative transfer. *Journal of Advances in Modelling Earth Systems* 15(5):e2022MS003445. <https://doi.org/10.1029/2022MS003445>
- Yousefi K, Hora G, Yang H, et al (2024) A machine learning model for reconstructing skin-friction drag over ocean surface waves. *Journal of Fluid Mechanics* 983(A9). <https://doi.org/10.1017/jfm.2024.81>
- Yuan Q, Shen H, Li T, et al (2020) Deep learning in environmental remote sensing: Achievements and challenges. *Remote Sensing of Environment* 241:111716. <https://doi.org/10.1016/j.rse.2020.111716>

[//doi.org/10.1016/j.rse.2020.111716](https://doi.org/10.1016/j.rse.2020.111716)

- Zaier I, Shu C, Ouarda TB, et al (2010) Estimation of ice thickness on lakes using artificial neural network ensembles. *Journal of Hydrology* 383(3-4):330–340. <https://doi.org/10.1016/j.jhydrol.2010.01.006>
- Zemp M, Chao Q, Han Dolman AJ, et al (2022) GCOS 2022 Implementation Plan. *Global Climate Observing System GCOS* (244):85
- Zhang L, Shao Z, Liu J, et al (2019) Deep learning based retrieval of forest aboveground biomass from combined LiDAR and Landsat 8 data. *Remote Sensing* 11(12):1459. <https://doi.org/10.3390/rs11121459>
- Zhang W, Gou J, Möller G, et al (2024) A new deep learning-assisted global water vapor stratification model for gnss meteorology: Validations and applications. *IEEE Transactions on Geoscience and Remote Sensing* <https://doi.org/10.1109/TGRS.2024.3479778>
- Zhang X, Liang F, Srinivasan R, et al (2009) Estimating uncertainty of streamflow simulation using Bayesian neural networks. *Water resources research* 45(2). <https://doi.org/10.1029/2008WR007030>
- Zhang Y, Long M, Chen K, et al (2023) Skilful nowcasting of extreme precipitation with nowcastnet. *Nature* 619(7970):526–532. <https://doi.org/10.1038/s41586-023-06184-4>
- Zheng A, Casari A (2018) *Feature engineering for machine learning: principles and techniques for data scientists.* ” O’Reilly Media, Inc.”
- Zhou K, Zheng Y, Dong W, et al (2020) A deep learning network for cloud-to-ground lightning nowcasting with multisource data. *Journal of Atmospheric and Oceanic Technology* 37(5):927–942. <https://doi.org/10.1175/JTECH-D-19-0146.1>
- Zhu XX, Tuia D, Mou L, et al (2017) Deep learning in remote sensing: A comprehensive review and list of resources. *IEEE geoscience and remote sensing magazine* 5(4):8–36. <https://doi.org/10.1109/MGRS.2017.2762307>
- Zhu XX, Xiong Z, Wang Y, et al (2024) On the Foundations of Earth and Climate Foundation Models. arXiv preprint arXiv:240504285 <https://doi.org/10.48550/arXiv.2405.04285>
- Zounemat-Kermani M, Batelaan O, Fadaee M, et al (2021) Ensemble machine learning paradigms in hydrology: A review. *Journal of Hydrology* 598. <https://doi.org/10.1016/j.jhydrol.2021.126266>